Horizontal and vertical interseismic velocity fields in the Vanuatu subduction zone from GPS measurements: Evidence for a central Vanuatu locked zone

N Bergeot, M Diament, Bruno Pelletier, M Régnier, S Calmant, V Ballu

Horizontal and vertical interseismic velocity fields in the Vanuatu subduction zone from GPS measurements: Evidence for a central Vanuatu locked zone

N. Bergeot,[1,2] M. N. Bouin,[3] M. Diament,[1] B. Pelletier,[4] M. Régnier,[5] S. Calmant,[6] and V. Ballu[1,4]

Received 28 June 2007; revised 28 November 2008; accepted 23 March 2009; published 23 June 2009.

[1] We analyzed interseismic velocity fields along the Vanuatu arc subduction zone from more than 45 GPS station measurements spanning 15 years. Convergence with respect to the Australian plate (AP) is normal to the trench, with amplitudes that vary greatly from a maximum of 170 mm a^{-1} at Vanikoro to 27 mm a^{-1} facing the D'Entrecasteaux Ridge (DER). Motions expressed relative to the Pacific plate (PP) highlight arc segmentation. Both the northern and southern segments undergo back-arc spreading in a roughly NE-SW direction, rotating anticlockwise and clockwise, respectively, while the central block moves eastward at a faster rate with respect to the PP than to the AP. More convergence is therefore accommodated at the eastern bound of the arc than at the Vanuatu trench. A right lateral strike-slip movement (26 ± 1 mm a^{-1}) along a zone normal to the trench (direction N70°) is necessary to accommodate the rate variation between the central and southern parts of the arc. Horizontal and vertical rates indicate partitioning between Malekula–southernmost Santo and central-northern Santo blocks. Simple elastic modeling of the interseismic stage deformation gives locked zone characteristics (25° dip and 50 km width) and a 54 mm a^{-1} long-term convergence rate between the AP and the central part of the Vanuatu arc from GPS horizontal and vertical velocities estimated south of the DER. The modeling does not fit the observed velocities facing the DER, probably because it does not account for the inelastic deformation associated with buoyant ridge subduction and back-arc thrusting.

Citation: Bergeot, N., M. N. Bouin, M. Diament, B. Pelletier, M. Régnier, S. Calmant, and V. Ballu (2009), Horizontal and vertical interseismic velocity fields in the Vanuatu subduction zone from GPS measurements: Evidence for a central Vanuatu locked zone, *J. Geophys. Res.*, *114*, B06405, doi:10.1029/2007JB005249.

1. Introduction

[2] Understanding the seismic cycle is a key step toward earthquake prediction. Strain accumulates during the interseismic stage between seismic events. Therefore, the interseismic motions must be monitored in order to understand the physical processes leading to the seismic rupture. The largest earthquakes mainly occur in subduction zones with strong coupling between plates. Strong interplate coupling in subduction zones is generally due to the presence of topographic structures like ridges or seamounts on the downgoing plate [*Cloos*, 1992]. In such a context, frequency of small or intermediate magnitude earthquakes is reduced and the probability of occurrence of large ($M_w > 8$) events increases [*Scholz and Small*, 1997].

[3] Several authors proposed models of interseismic velocity field [e.g., *Nur*, 1974; *Savage and Prescott*, 1978; *Bourne et al.*, 1998] but very few document the effects of ridge collision on the interseismic stage. *Geist et al.* [1993], using a thin viscous sheet model, studied the influence of the subduction ridge on the long-term vertical deformation. Short-term vertical deformations are still poorly understood because short-term vertical displacements are difficult to measure. Moreover, in the case of oceanic arcs, the use of space geodesy techniques (Global Navigation Satellite System (GNSS), interferometric synthetic aperture radar (InSAR)) is limited by the sparse distribution of small islands that prevent the setup of optimum designed networks.

[4] Arc-ridge collisions in a subduction zone are quite common (e.g., Lesser Antilles, Sumatra, South America, Japan, and southwest Pacific). This article focuses on the short-timescale (15 years) effects of a ridge entering a

[1]Equipe de Géophysique Spatiale et Planétaire, Institut de Physique du Globe de Paris, UMR 7154, CNRS Université Paris Diderot, Paris, France.
[2]Now at Reference Systems and Geodynamic, Royal Observatory of Belgium, Brussels, Belgium.
[3]Laboratoire de Recherches en Géodésie, Institut Géographique National, Champs sur Marne, France.
[4]Géosciences Azur, UMR 6526, IRD, Nouméa, New Caledonia.
[5]Géosciences Azur, UMR 6526, IRD, Valbonne, France.
[6]Laboratoire d'Etudes en Géophysique et Océanographie Spatiales, UMR 5566, Observatoire Midi Pyrenées, CNRS, Toulouse, France.

0148-0227/09/2007JB005249$09.00

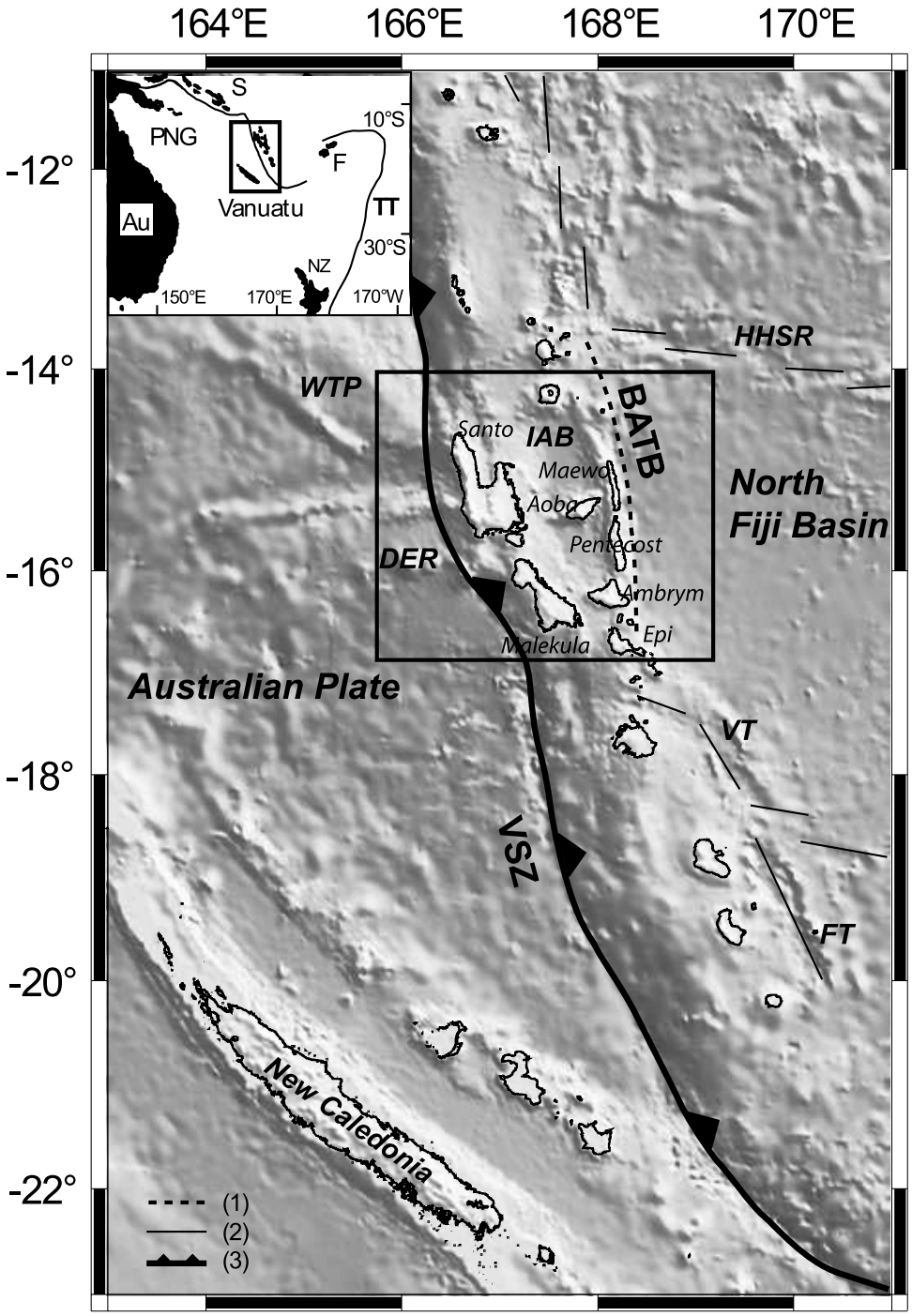

Figure 1. Map of the study area in the southwest Pacific. Dashed line is the back-arc thrust belt (BATB); solid lines are the spreading ridge; bold line is the Vanuatu subduction zone (VSZ). Bathymetry data are from *Calmant et al.* [2002]. The black rectangle is the central part of the Vanuatu arc. Abbreviations are as follows: DER, D'Entrecasteaux Ridge; WTP, West Torres Plateau; IAB, Intra-arc Basin; HHSR, Hazel Holme spreading ridge; FT, Futuna Trough; VT, Vate Trough. (top left) Regional map. Abbreviations are as follows: Au, Australia; NZ, New Zealand; TT, Tonga Trench; S, Salomon Islands; PNG, Papua New Guinea; F, Fiji Island. The black rectangle is the study area (corresponding to the main figure) and the solid line is the trench.

subduction zone with high convergence rates and vertical deformation. In the central part of the Vanuatu subduction zone (Figure 1), the interaction of the D'Entrecasteaux Ridge (DER) with the arc [*Chung and Kanamori*, 1978; *Isacks et al.*, 1981; *Collot et al.*, 1985] strongly increases the plate coupling and yields significant variations in the horizontal velocity along the converging boundary [*Pelletier and Louat*, 1989; *Calmant et al.*, 1995, 2003;

Taylor et al., 1995]. Presence of several parallel chains of islands at various distances from the trench allows us to monitor the short-term deformation field across the entire convergent margin using space geodesy (GPS) techniques. Our goal here is to map and discuss the strain field along the subduction zone, especially in the locked area, which may generate large seismic events. To this end, we document both the horizontal and vertical components of the surface displacements during the interseismic stage of the seismic cycle. These velocities are of the order of a few mm a^{-1} for the vertical and a few cm a^{-1} for the horizontal. The GPS vertical component is about one third as precise as the horizontal components in a local network with baseline lengths less than 450 km [*Larson and Agnew*, 1991]. To reduce the reference system errors on the vertical component, we use the combination strategy developed for the realization of the International Terrestrial Reference Frame (ITRF) [*Altamimi et al.*, 2002, 2007].

2. Geodynamic Setting

[5] The Vanuatu subduction zone (VSZ) is located in the southwestern Pacific and extends about 1500 km between 11° and 23°S (see Figure 1). Along this converging boundary, the Australian plate (AP) subducts beneath the Vanuatu arc and the North Fiji Basin (NFB) spreading area [*Auzende et al.*, 1995]. The Vanuatu trench averages more than 6000 m depth except between 14° and 17°S, where the trench disappears facing the DER and the West Torres Plateau (WTP), the two high topographic features on the AP. The DER started subducting under the arc 2–3 Ma ago [*Collot et al.*, 1992; *Greene et al.*, 1994] while the WTP probably started subducting more recently (0.7–1 Ma, [*Meffre and Crawford*, 2001]).

[6] The convergence rates of the Vanuatu trench with respect to the AP are estimated to be between 30 and 40 mm a^{-1} in the DER and WTP and between 90 and 170 mm a^{-1} in the other segments of the subduction [*Dubois et al.*, 1977; *Louat and Pelletier*, 1989; *Pelletier and Louat*, 1989; *Calmant et al.*, 1995, 2003; *Taylor et al.*, 1995; *Pelletier et al.*, 1998]. This large variation in the convergence rate is accommodated by active deformation in both the Vanuatu arc and the back-arc North Fiji Basin. The morphology, seismicity and convergence vectors indicate than the VSZ is divided into 3 blocks [*Calmant et al.*, 2003]: (1) a north block (10°–13°S) including the Banks and Torres islands, which rotates counterclockwise with respect to the NFB; (2) a south block (17°–21°S) which rotates clockwise with respect to the NFB; and (3) a central block (13°–17°S) which translates eastward toward the NFB (Figure 2). The translation of the central block toward the NFB is accommodated by a zone of intra-arc shortening and possibly initiation of a west dipping subduction along the eastern side of the back-arc thrust belt (BATB) that thickens the crust [*Collot et al.*, 1985; *Lagabrielle et al.*, 2003; *Régnier et al.*, 2003].

[7] The central block islands can be split into three sets according to their geology [*Mitchell and Warden*, 1971; *Mallick*, 1975; *Carney and MacFarlane*, 1982; *Carney et al.*, 1985; *MacFarlane et al.*, 1988] and geodynamic setting (see Figure 3 for island names). The western islands, Santo and Malekula, are composed of upper Oligocene–lower Miocene arc-related volcanic rocks, upper Miocene to Pleistocene sediments and Quaternary coral reef limestones. They result from long-term (Quaternary) and complex uplift of the seafloor in response to the DER subduction. The Holocene uplift estimated from measurements of emerged corral reefs reaches 6 mm a^{-1} on south Santo and 3 mm a^{-1} on NW Malekula [*Jouannic et al.*, 1980; *Taylor et al.*, 1980, 1985, 1987, 1990]. The eastern belt (Maewo and Pentecost islands) is characterized by upper Miocene subaerial to submarine volcanism. These islands are uplifted consequently to the crust shortening on the BATB. Aoba Island in the center of the Intra Arc Basin (IAB), Gaua Island in the north and Ambrym Island in the south are active volcanoes.

[8] The longest recurrence interval between large earthquakes is estimated to be 375 years in the south Pentecost-Ambrym segment of the back-arc area [*Lagabrielle et al.*, 2003]. The recurrence interval varies from 50 to 400 years in the three fore arc segments of the central Vanuatu block [*Taylor et al.*, 1990]. The shortest interval in the south Santo segment reflects intense geodynamic activity in the region and invites further investigations. We focus on this locked part of the VSZ to characterize the arc deformation due to ridge subduction and to better understand the effect of a ridge on the interseismic deformation. To this end, we monitored the horizontal and vertical velocity fields over the entire arc between 1992 and 2006 using permanent and revisited GPS stations.

3. Data Processing

[9] Previous studies using GPS data in the area [*Taylor et al.*, 1995; *Calmant et al.*, 1995, 1997, 2003] quantified the global horizontal velocity field. Our goal here was to homogeneously resolve both vertical and horizontal velocity fields with larger time series from 10 to 15 years. We reprocessed all the available GPS data (1992–2003) and new GPS data of 2004 to 2006 using a state-of-the-art free network strategy. We paid special attention to GPS modeling (e.g., antenna phase center variations, atmospheric effects) and to reference system issues that impact the vertical component accuracy.

3.1. GPS Network

[10] The first data we used were collected in 1992 during the U.S. Southwest Pacific GPS project (SWPP) [*Schutz et al.*, 1993]. From 1992 to 2004, the data were collected by the Institut pour la Recherche et le Développement (IRD) and SWPP teams on Vanuatu and New Caledonia islands with Choke Ring antennas and dual frequencies receivers. More than fifty geodetic sites were reoccupied on a regular base from 1992 to 2002 and nearly each year since then. Five continuous GPS stations (KOUC, LPIL, SANC, VILA, NOUM; see Figure 3) were installed between 1996 and 1997 on the AP and Vanuatu archipelago. They were maintained in collaboration with the Vanuatu Geodetic Survey Dept. in Vanuatu and with the Direction des Infrastructures de la Topographie et des Transports Terrestres/Bureau de Géodésie et Nivellement (DITTT/BGN) in New Caledonia. A sixth continuous GPS station started operating in 2002 on the west coast of Santo Island (TGWS; see Figure 3). We measured 28 GPS sites in 2004, 2005 and

2006 on the central Vanuatu network to lengthen the time series and reduce the effect of seasonal variations (hydrological and atmospheric loading) on the velocity estimation. Indeed, more than 2.5 years of GPS observations are needed in order to reduce the effect of seasonal variations [*Blewitt and Lavallée*, 2002]. To avoid antenna height measurement errors, we used especially designed constant height geodetic masts that are also more stable than tripods. Most of the sites were measured during at least three 24-h sessions during each experiment. We have now ~1300 daily GPS

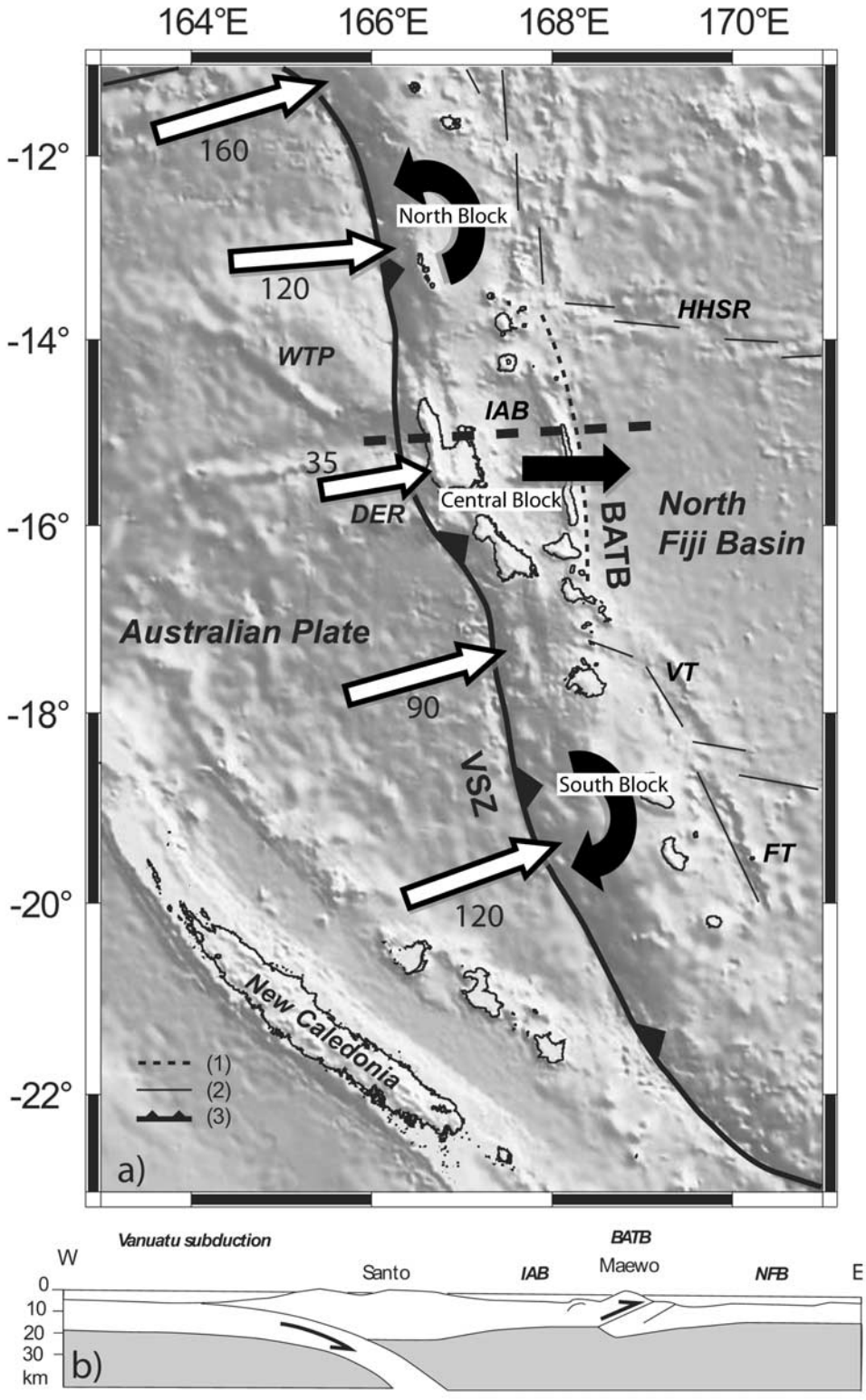

Figure 2

data from revisited stations along the Vanuatu arc between 1992 and 2006.

3.2. Processing Strategy and Reference Settings

[11] To ensure the reference frame realization in a homogeneous way, we included our Vanuatu sites in a global network (Figure 4). This keeps the transformation parameters estimation free of high correlations, especially between translation corresponding to local height direction and scale factor. We selected 30 International GNSS Service (IGS) stations out of the 93 IGb00 reference tracking sites (see http://igscb.jpl.nasa.gov/mail/igsmail/2003/msg00441.html, http://igscb.jpl.nasa.gov/mail/igsstation/2005/msg00035.html, ftp://macs.geod.nrcan.gc.ca/pub/requests/sinex/discontinuities). Our selection criteria are based on station installation epoch (since our experiment started in 1992 with a very sparse IGS network), geographic situation (to obtain a global distribution within the network) and station quality (according to http://igscb.jpl.nasa.gov/mail/igsmail/2003/msg00441.html, ftp://macs.geod.nrcan.gc.ca/pub/requests/sinex/discontinuities). Baseline lengths range from a few km within our local network to more than 12,000 km, especially early on in the experiment due to the lack of permanent stations in the Pacific region.

[12] We computed positions using the GAMIT 10.1 software [*King and Bock*, 2003]. Twenty-four-hour measurement sessions are reduced to daily positions using the ionosphere-free combination and fixing the ambiguities to integer values. We used precise orbits from the IGS [*Beutler et al.*, 1999] and Earth Orientation Parameters from the International Earth Rotation Service (IERS) B Bulletin. We applied solid Earth and polar tide corrections following the latest IERS standards [*McCarthy and Petit*, 2004] and ocean loading corrections using the eight principal components of the CSR4.0 ocean tide model [*Eanes and Schuler*, 1999] computed on an elastic Earth model (see http://www.oso.chalmers.se/~loading/). We also used tables provided by the IGS for relative modeling of antenna phase center variations. We estimated tropospheric delay parameters (one every hour) using the Saastamoinen modeling for a priori values [*Saastamoinen*, 1973a, 1973b, 1973c] and the standard Niell Mapping Function [*Niell*, 1996]. The atmospheric gradient estimation is known to improve atmospheric modeling at global scale as well as the positioning precision [*Walpersdorf et al.*, 2001]. They were estimated once a day in the NS and EW directions. The elevation cutoff angle was set to 7° as a trade-off between the ratio observation/parameter number and the validity of atmospheric modeling at low elevation angles. We used a free network processing strategy with constraints on the IGS00 a priori positions of 20 to 50 cm, obtaining unconstrained daily solutions for our stations.

[13] A key aspect of this study is the long-term (more than 13 years) consistency of the reference frame realization within our solution. In order to avoid systematic effects (especially on the vertical component), we combine our individual solutions with a reference frame realization in a rigorous way. In this prospect, we used the combination strategy developed by *Altamimi et al.* [2002] to process the multitechnique Reference Frame realization ITRF2000. The CATREF software [*Altamimi et al.*, 2002] uses the minimal constraints approach to simultaneously estimate the position and the velocity for each site of the network as well as 7 position transformation parameters between each individual daily solution and the combined solution. This least squares estimation is weighted using the full variance-covariance matrix of every daily solution. The minimal constraints approach is implemented by imposing the 7 + 7 parameter transformation between the combined solution and the reference frame (in our case IGS00) to be zero (no global translation, rotation or scale factor, no time derivatives of these quantities). The final positions and velocity field are therefore expressed into the chosen (IGS00) reference frame. We chose the IGS00 reference frame (see http://igscb.jpl.nasa.gov/mail/igsmail/2003/msg00441.html) rather than ITRF2000 for two main reasons. First, the ITRF release we used includes data until 2000 only. Some IGS sites, especially in the Pacific area, were poorly determined in position and velocity at this time. The IGS00 realization is regularly updated by including IGS analysis center combined weekly solutions. Its velocity field (especially on the vertical component) is therefore more accurate. Second, the IGS reference is based on GPS solutions only. This ensures a greater consistency for individual GPS experiments (as already shown by http://igscb.jpl.nasa.gov/mail/igsmail/2003/msg00441.html). The IGS precise orbit processing is based on this reference frame realization, which is in addition aligned on ITRF2000 for the datum definition.

[14] From this preliminary solution, we estimated a variance factor σ_i^2 for each daily solution i. This variance factor is then applied to the covariance matrix of the corresponding daily coordinate set in an iterative way until the global a posteriori variance factor equal unity. This ensures the resulting formal errors of the combined solutions (e.g., vertical velocity standard deviations) to be representative of the formal errors on the sites before the combination.

[15] We used a statistical test to reject any individual solution of revisited stations with a position normalized RMS (nrms) greater than 3 with respect to the combined position at the same epoch. This guarantees that the velocity estimation will not be influenced by poor GPS observation conditions like short sessions, bad quality data, wildlife or

Figure 2. (a) Geodynamic setting of the VSZ, with block motions relative to the North Fiji Basin [from *Calmant et al.*, 2003]. The Vanuatu arc is split into three blocks, with anticlockwise rotation (north), convergence (center), and clockwise rotation (south). Dashed line is the BATB; solid lines are the spreading ridge; bold line is the VSZ. Bathymetry data are from *Calmant et al.* [2002]. The black rectangle is the central part of the Vanuatu arc. White arrows are velocities (millimeters per year) with respect to the Australian plate (AP); black arrows are block motion with respect to the North Fiji Basin. Dotted line is the cross section of Figure 2b. (b) Schematic of the central part of the VSZ [from *Lagabrielle et al.*, 2003]. The direction of this cross section is west to east, and it intersects the Santo and Maewo Islands (dotted line in Figure 2a). Abbreviations are as follows: IAB, Aoba Intra-arc Basin; BATB, back-arc thrust belt; NFB, North Fiji Basin.

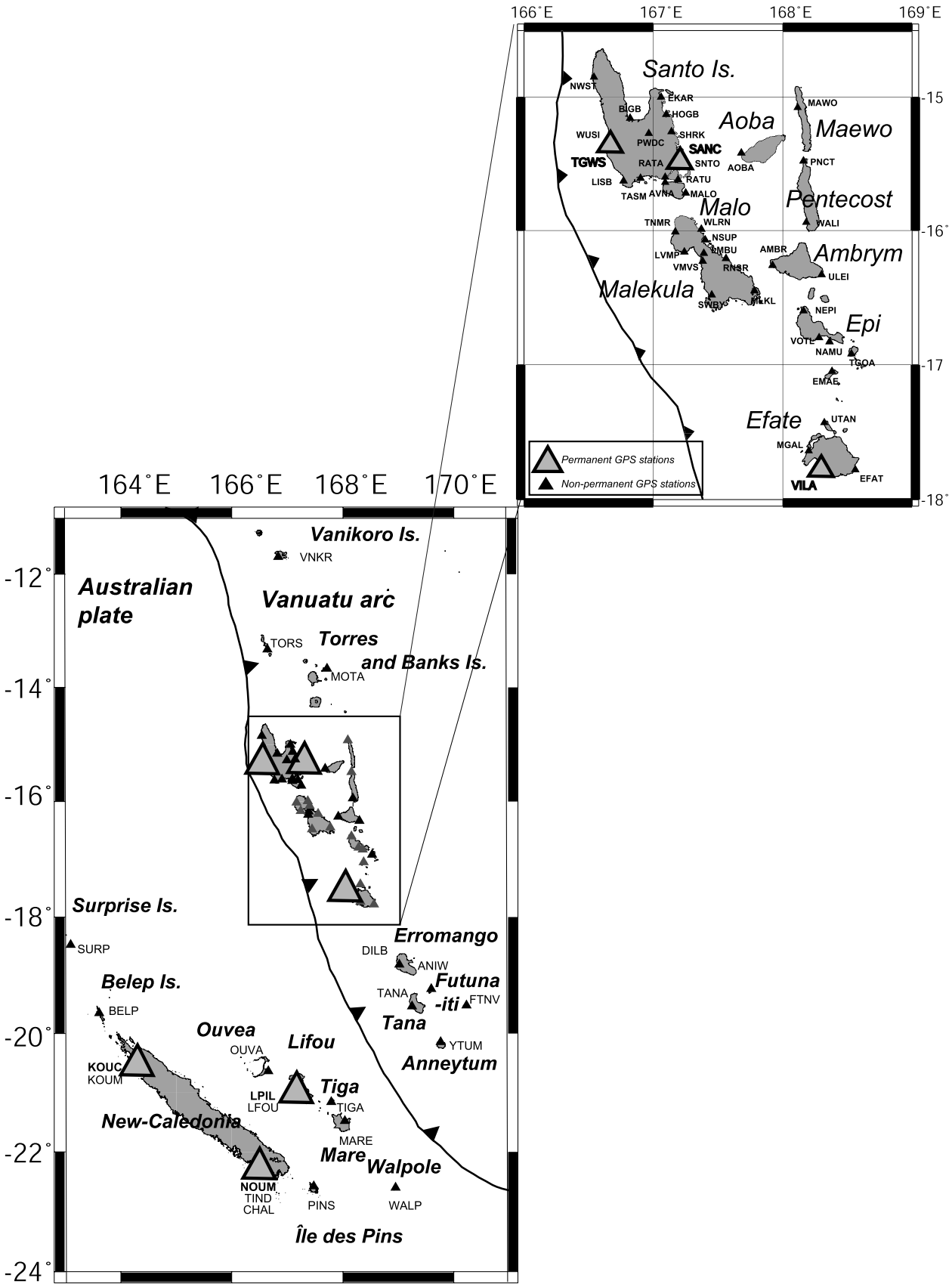

Figure 3. Local GPS network used in this study. The Vanuatu central block, with dense network, is enlarged in the upper right corner. Large triangles are for the permanent sites.

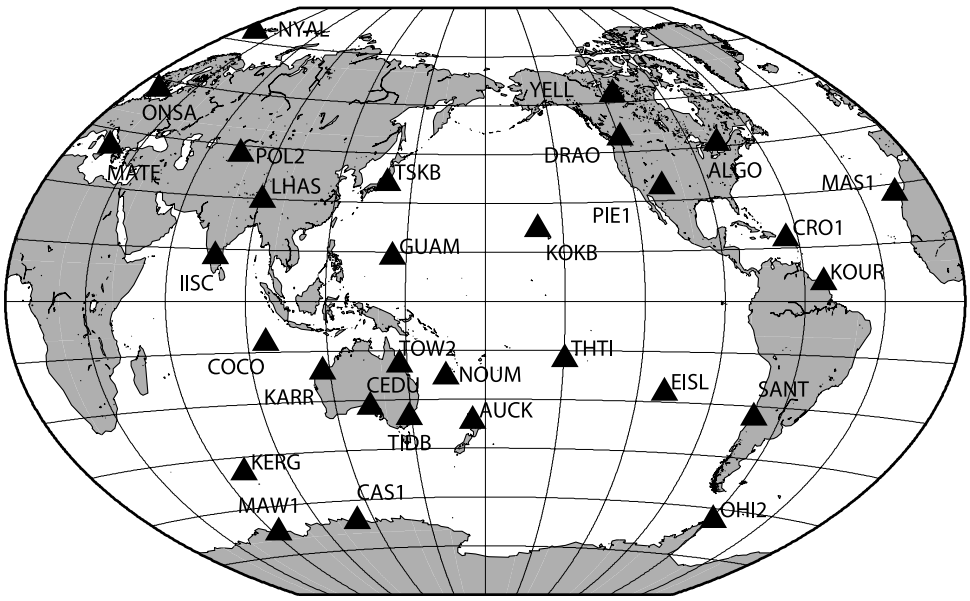

Figure 4. International GNSS Service (IGS) GPS station network used for defining our reference system (30 stations in addition to the local network).

human antenna disturbance. On the whole experiment, 58 sites × days were rejected as outliers, representing ∼4% of the data. The reference setting is iterated after this post processing to obtain our final results. The 3-day repeatability (i.e., the RMS of the positions with respect to the average value on a given component for a 3-day measurement length) on the campaign stations is then less than 2 mm on each component. Finally, we estimated the overall positioning precision on the permanent stations by computing the 10-day repeatability: we obtain 2 to 3 mm on the north component, 4 mm for the east component and 5 to 9 mm for the height.

[16] As already stated, the Vanuatu archipelago is an active seismologic zone with strong recurrent shallow earthquakes of magnitude larger than or equal to 7 (e.g., 1994 on Efate and on SW Malekula; 1999 on Ambrym; 2000 on Santo and 2002 on Efate). Our GPS time series show coseismic steps and several GPS stations were affected by up to 3 coseismic displacements during the length of observation. For instance, Figure 5 shows time series of the east component on a permanent GPS station (SANC) and on a revisited GPS station (HOGB) at the east of Santo Island. Both series present two coseismic offsets due to the Ambrym 1999 and Santo 2000 earthquakes. The CATREF software provides estimation of coseismic steps within the time series. During the reference setting we compute positions before and after each earthquake and we force the site velocity to be the same before and after the seismic event. It does not account for postseismic relaxation: the station position is assumed to behave linearly and constant during interseismic period between every coseismic displacement. We used this option to estimate coseismic steps and interseismic velocities at each GPS station when coseismic displacements are identified in the time series, for the 1994 Malekula, 1999 Ambrym, 2000 Santo and 2002 Efate earthquakes. An example of the resulting time series with linear interseismic velocities and coseismic steps estimated are shown in Figure 5.

3.3. GPS Result Validation

[17] To validate the GPS data processing, especially the estimation of the vertical velocity, we performed two comparisons, as follows.

[18] 1. We performed a comparison of CGPS velocities with IGb00 velocity field. To assess the consistency of our results within the IGS00 reference frame, we compared our horizontal velocities on all available permanent GPS stations with the IGb00 (see http://igscb.jpl.nasa.gov/mail/igsmail/2003/msg00441.html) velocities (Table 1). The agreement is generally better than 1 mm a^{-1} on every component. Residuals remain under 2 mm a^{-1} for every station on the east and north component. Larger residuals on the up component (e.g., KOKB station, 4 mm a^{-1}) can be explained by the isolated location of this station in the middle of the Pacific Ocean as well as by the different time spans considered (2000–2004 for IGS00, 1990–2005 for this study and KOKB station).

[19] 2. We performed a Euler pole estimation. We estimated best fit Euler pole for the AP and Pacific plate (PP) and relative Australian/Pacific motion from our horizontal velocity field and compare the results with those from previous studies (Table 2). Only CGPS stations with series longer than 5 years were used for these pole computations. The velocity residuals of the stations used (8 for the AP, 6 for the PP) are less than 2 mm a^{-1}, 3 mm a^{-1} respectively. Our results show very good agreements (less than 2° discrepancy for the pole location, 0.02° Ma^{-1} for the velocity for the AP, 0.5° for the pole location and 0.01° Ma^{-1} for the rate for the PP) with previous studies based on different data sources: combination of geodetic techniques (ITRF2000 [*Altamimi et al.*, 2002]), GPS [*Calmant et al.*, 2003; *Beavan et al.*, 2002], and geomagnetic and seismic data analysis [*DeMets et al.*, 1994].

[20] These tests show that the horizontal and vertical velocity fields computed for both permanent and campaign

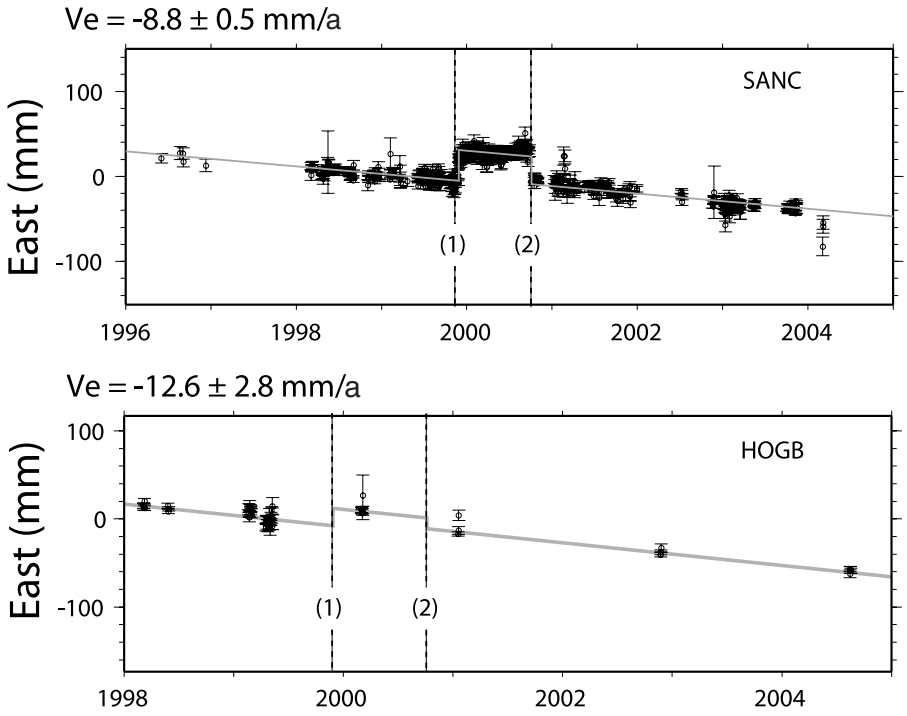

Figure 5. GPS time series of the (top) east component of Santo (SANC) permanent station and (bottom) one (HOGB) revisited station. Each of the time series presents two coseismic displacements. Dotted lines are (1) Ambrym, 1999, and (2) Santo, 2000, earthquakes. The shaded line and Ve are the interseismic velocity as estimated by the CATREF software.

stations in our network are accurately determined. It can be thus used to map the interseismic deformation in the VSZ.

4. Results and Discussion

[21] We now present and discuss our results on the interseismic convergence rate variations along the trench as well as on the motions relative to a NFB fixed reference frame following the *Calmant et al.* [2003] motion representation. We then infer the 3-D velocities field for the central block and use them to estimate the size and position of the locked zone interface as well as the long-term convergence rate between the AP and the Vanuatu arc using a simple elastic model [*Savage*, 1983].

4.1. Convergence Along the Vanuatu Trench and Along-Strike Variations

[22] Table 3 and Figure 6 present the horizontal velocities derived from our GPS analysis with respect to the AP as modeled from our global velocity field (see explanation above) for all the stations in the vicinity of the Vanuatu arc. Our solution is based on longer (until 2005) time series than that of *Calmant et al.* [2003] for most sites and includes 10 additional sites that were not sufficiently constrained for their study. As in the work of *Calmant et al.* [2003], convergence vector vary greatly in magnitude along the trench and are nearly always normal to the trench.

[23] Facing the DER, roughly between 14.5°S and 16.5°S, horizontal velocities are significantly reduced and are even less than the motion between the AP and PP (more than 80 mm a^{-1} N260° at location −16° latitude, 167° longitude from the NUVEL-1A [*DeMets et al.*, 1994] Australian/Pacific relative plate motion model). For all stations, the velocities are consistent in magnitude and orientation (between 25 and 43 mm a^{-1}, N240° and N255°) with the exception of the sites in the close vicinity of the BATB, east of the Aoba Intra Arc Basin (Maewo and Pentecost), where velocities are about 54–56 mm a^{-1} (Figure 6). The lowest rates (25 to 31 mm a^{-1}) are found at sites close to the trench, along the western coast of Santo and Malekula. These results indicate that the motion along the subduction plane is locked in this part of the Vanuatu trench and the entire arc itself undergoes significant deformation.

[24] South of the DER, the velocities increase regularly, reaching 80 ± 10 mm a^{-1} in the Epi/Tongoa area, 90 ± 5 mm a^{-1} around Efate and 120 ± 5 mm a^{-1} at the southernmost part of the study area (Tanna/Aneytum; see Figure 3 for island names). This variation possibly reflects the decreasing influence of the DER subduction/collision. Except at the easternmost sites of Futuna-Iti (FTNV) and Tongoa (TGOA) the orientation of the convergence is consistent. Since FTNV and TGOA show significant discrepancies in velocity direction with respect to stations located to their west, we infer interaction between tectonic discontinuities and FTNV and TGOA sites belong to the NFB, that is to one of the platelets stuck between the Vanuatu arc and the PP, as suggested previously by *Pelletier and Louat* [1989] and *Calmant et al.* [2003].

[25] The four stations west of TGOA (NEPI, VOTL, NAMU, and EMAE; see Table 3 and Figures 3 and 6 for station names) define a transition zone between the central block with lower convergence rates and the southern block with high and increasing southward velocities.

Table 1. Velocity Residuals on the IGS00 Sites With Respect to IGS00 Velocities

	Longitude (deg)	Latitude (deg)	Differences (mm a^{-1}) East	North	Up
		African Plate			
MAS1	−15.63	27.76	0.1	−0.5	−0.1
		Antarctica Plate			
CAS1	110.52	−66.28	−0.3	0.0	−1.8
KERG	70.26	−49.35	0.0	0.3	−4.0
MAW1	62.87	−67.6	−0.1	0.0	−1.7
OHI2	−57.9	−63.32	−0.8	3.2	0.5
ONSA	11.93	57.4	0.0	−0.4	0.8
		Australian Plate			
AUCK	174.83	−36.6	−0.6	0.7	1.4
CEDU	133.81	−31.87	0.9	0.6	1.4
COCO	96.83	−12.19	8.0	−0.9	−0.5
KARR	117.1	−20.98	0.2	1.1	−0.1
NOUM	166.41	−22.27	−0.2	−0.3	−1.6
TIDB	148.98	−35.4	0.3	0.1	1.8
TOW2	147.06	−19.27	0.9	0.8	0.7
		Caribbean Plate			
CRO1	−64.58	17.76	−0.4	−0.2	4.1
		Eurasia Plate			
LHAS	91.1	29.66	−0.8	0.0	1.6
MATE	16.7	40.65	0.4	−0.2	−0.5
NYAL	11.87	78.93	−0.1	−0.8	−0.2
POL2	74.69	42.68	−0.1	0.4	1.2
TSKB	140.09	36.11	0.7	0.4	−0.7
		Indian Plate			
IISC	77.57	13.02	−0.1	0.6	2.4
		Nazca Plate			
EISL	−109.38	−27.15	−0.1	−0.5	0.2
		North American Plate			
DRAO	−119.62	49.32	0.6	0.0	−0.6
PIE1	−108.12	34.3	0.7	0.3	−0.2
STJO	−52.68	47.6	0.0	−0.3	−1.5
YELL	−114.48	62.48	0.8	0.0	−1.0
		Pacific Plate			
KOKB	−159.66	22.13	−3.0	−3.5	−4.4
THTI	−149.61	−17.58	−1.5	0.7	3.0
		Philippine Plate			
GUAM	144.87	13.59	1.2	−2.4	−1.1
		South American Plate			
KOUR	−52.81	5.25	0.5	0.1	−2.2
SANT	−70.67	−33.15	0.3	−0.5	2.7

[26] There are only three stations north of Santo, preventing any detailed analysis. The northernmost one, Vanikoro, Salomon Islands, shows the highest convergence rate along the arc (172 ± 36 mm a^{-1}). This velocity, one of the largest observed between neighboring plates, is in very good agreement with the convergence rate of 160–170 mm a^{-1} oriented N245 ± 5° predicted at 11°S by *Pelletier and Louat* [1989] and *Pelletier et al.* [1998] from geodynamic considerations. On Banks and Torres Islands (MOTA, TORS), the convergence rate of 70 ± 11 mm a^{-1} is close to the value predicted from the Australian/Pacific plate motion. Finally, the Torres (TORS) velocity orientation (N244 ± 8°) significantly differs from normal to the trench. However, the motions at these three sites are determined with large uncertainties since determined using only two to three measurement campaigns, due to their remote location (1998 and 1999 for Banks and Torres sites, 2003 and 2005 for VNKR).

4.2. Motions Relative to the North Fiji Basin: Block Rotations and Arc Segmentation

[27] We derive the horizontal velocities of all our sites with respect to a PP-fixed reference frame. We assume here that the NFB motion is undistinguished from that of the PP rotation. Indeed, the west North Fiji Basin microplate is separated from the PP by a very slow (maximum 15 to 20 mm a^{-1}) spreading axis [*Pelletier and Louat*, 1989; *Louat and Pelletier*, 1989; *Pelletier et al.*, 1998; *Calmant et al.*, 2003]. This axis, the E-W trending Hazel Holme spreading ridge (see Figure 1 for location), vanishes westward and abuts the Vanuatu arc near 13.5°S. The velocities expressed relative to the PP rigid motion (as estimated in the previous section; see Table 2) are presented in Table 3 and Figure 7. GPS horizontal velocities of the Vanuatu arc relative to the PP show large variations. We can identify three different domains: the first one contains the three northernmost stations, the second one containing stations located on Santo, Malekula, and the eastern belt of the Aoba Basin and the third one includes the stations from Epi to Aneytum.

[28] Previous studies [*Pelletier and Louat*, 1989; *Pelletier et al.*, 1998; *Calmant et al.*, 2003] suggested that the arc is segmented in three blocks corresponding roughly to our three domains. We now discuss our results in light of this segmentation.

[29] As far as the northern part is concerned, although the number of sites is limited, some conclusions can be drawn. If we assume that the three sites belong to a unique block, we can assess a rigid block rotation for these three stations using a least squares inversion (see Figure 7 and Table 4). The modeled velocities fit the data within the error bars but, due to the limited number of sites, no definite conclusion can be drawn. However, the three sites may belong to different blocks. The northernmost site of Vanikoro espe-

Table 2. Comparison of Euler Poles Determined in This Study for the Australian and Pacific Plate Absolute Motions and the Relative Australian/Pacific Plate Motion With Results of Previous Studies

	Longitude (deg), Latitude (deg), Velocity (deg Ma^{-1})
Australian Plate	
This study	37.10, 32.10, 0.622
Calmant et al. [2003]	37.84, 32.15, 0.607
Altamimi et al. [2002]	39.40, 32.30, 0.614
Beavan et al. [2002]	37.54, 32.76, 0.621
Pacific Plate	
This study	110.50, −64.13, 0.667
Calmant et al. [2003]	111.15, −63.40, 0.676
Altamimi et al. [2002]	110.19, −64.17, 0.676
Beavan et al. [2002]	110.86, −63.75, 0.677
Australian/Pacific Plate Motion	
This study	185.10, −61.4, 1.073
Calmant et al. [2003]	183.89, −60.62, 1.061
DeMets et al. [1994]	181.70, −60.1, 1.070
Beavan et al. [2002]	184.19, −61.04, 1.078

Table 3. GPS Horizontal Velocities for the Sites of the Vanuatu Subduction Zone Related to the Australian Plate Rigid Motion and Related to the Pacific Plate Motion as Estimated From Our GPS Rates[a]

			Australian Plate Fixed Rigid Motion		Pacific Plate Fixed Rigid Motion	
Site	Longitude (deg)	Latitude (deg)	Direction (deg)	Velocity (mm a^{-1})	Direction (deg)	Velocity (mm a^{-1})
			North Block			
VNKR	166.84	−11.69	N246.6 ± 25.3	172.0 ± 35.6	N232.4 ± 28.3	84.4 ± 41.3
TORS	166.64	−13.33	N224.4 ± 8.2	72.0 ± 4.3	N130.6 ± 10.9	52.0 ± 5.3
MOTA	167.72	−13.67	N262.9 ± 9.8	70.1 ± 11.4	N68.4 ± 43.8	21.3 ± 12.4
			Central Block			
Santo/Malo						
NWST	166.54	−14.85	N244.6 ± 2.2	27.3 ± 1.2	N84.6 ± 0.8	63.4 ± 1.3
WUSI	166.66	−15.36	N254.8 ± 1.3	37.4 ± 1.2	N81.4 ± 1.0	51.3 ± 1.3
TGWS[b]	166.66	−15.36	N253.4 ± 0.9	43.1 ± 1.0	N83.9 ± 0.9	45.1 ± 1.1
LISB	166.77	−15.63	N247.2 ± 1.7	31.0 ± 1.2	N84.7 ± 0.8	58.3 ± 1.2
TASM	166.9	−15.61	N243.5 ± 1.6	32.4 ± 1.1	N87.4 ± 0.7	57.3 ± 1.1
AVNA	167.09	−15.64	N243.2 ± 2.3	32.3 ± 1.4	N87.6 ± 0.9	57.6 ± 1.3
RATA	167.09	−15.6	N252.3 ± 2.8	34.4 ± 1.9	N83.0 ± 1.6	54.0 ± 1.8
RATU	167.19	−15.62	N249.0 ± 2.2	38.0 ± 1.8	N86.2 ± 1.2	51.3 ± 1.8
MALO	167.25	−15.72	N249.7 ± 2.4	33.2 ± 1.8	N84.4 ± 1.2	55.4 ± 1.7
SNTO	167.2	−15.45	N243.6 ± 0.9	39.2 ± 0.8	N90.7 ± 0.6	51.4 ± 0.9
SANC[b]	167.2	−15.45	N246.9 ± 0.4	38.4 ± 0.3	N87.8 ± 0.5	51.3 ± 0.7
SHRK	167.14	−15.26	N247.8 ± 3.6	42.4 ± 3.6	N88.8 ± 2.0	47.2 ± 3.4
HOGB	167.1	−15.13	N248.6 ± 1.2	42.3 ± 1.2	N88.0 ± 0.9	47.4 ± 1.2
EKAR	167.06	−15.00	N247.5 ± 1.7	39.1 ± 1.5	N87.9 ± 1.0	50.3 ± 1.5
BIGB	166.82	−15.16	N247.6 ± 1.6	37.4 ± 1.3	N86.6 ± 0.9	52.4 ± 1.4
Aoba						
AOBA	167.68	−15.42	N249.4 ± 2.9	38.4 ± 2.7	N86.8 ± 1.6	50.3 ± 2.4
Maewo						
MAWO	168.08	−15.08	N254.1 ± 0.8	56.2 ± 1.2	N88.7 ± 1.3	33.3 ± 1.3
Pentecost						
PNCT	168.16	−15.48	N262.6 ± 0.8	54.1 ± 1.1	N74.5 ± 1.7	34.4 ± 1.3
WALI	168.18	−15.94	N277.4 ± 7.5	17.4 ± 3.5	N74.9 ± 2.3	70.4 ± 3.8
Malekula						
TNMR	167.17	−16.01	N251.8 ± 2.9	31.0 ± 1.8	N82.6 ± 1.4	57.2 ± 1.8
LVMP	167.24	−16.16	N249.0 ± 2.7	25.4 ± 1.4	N82.9 ± 1.0	62.3 ± 1.4
VMVS	167.38	−16.23	N250.5 ± 3.1	25.3 ± 1.7	N82.3 ± 1.1	62.2 ± 1.3
SWBY	167.45	−16.48	N254.1 ± 1.9	25.2 ± 1.0	N80.9 ± 0.8	61.4 ± 1.2
MLKL	167.78	−16.45	N249.3 ± 1.3	41.2 ± 1.1	N87.6 ± 0.9	47.0 ± 1.1
RNSR	167.56	−16.21	N253.6 ± 1.2	31.1 ± 0.8	N82.1 ± 0.8	55.3 ± 1.0
LMBU	167.39	−16.17	N252.2 ± 2.3	28.4 ± 1.4	N82.2 ± 1.1	59.1 ± 1.4
NSUP	167.4	−16.07	N244.2 ± 2.6	25.3 ± 1.3	N84.8 ± 0.9	63.3 ± 1.3
WLRN	167.37	−15.99	N250.4 ± 1.8	30.2 ± 1.2	N83.4 ± 0.9	57.4 ± 1.2
Ambrym						
AMBR	167.92	−16.26	N240.1 ± 1.8	35.3 ± 1.3	N91.6 ± 0.8	54.3 ± 1.3
ULEI	168.3	−16.33	N251.5 ± 1.3	48.4 ± 1.5	N89.2 ± 1.3	39.4 ± 1.4
			South Block			
Epi/Tongoa						
NEPI	168.16	−16.6	N233.2 ± 2.1	62.0 ± 2.4	N120.6 ± 3.1	41.4 ± 2.3
VOTL	168.28	−16.8	N233.5 ± 0.6	73.4 ± 0.8	N137.2 ± 1.6	37.4 ± 1.1
NAMU	168.36	−16.83	N232.8 ± 1.5	76.3 ± 2.2	N142.7 ± 3.4	38.3 ± 2.2
TGOA	168.53	−16.92	N252.1 ± 0.5	86.4 ± 0.9	N169.3 ± 5.4	11.1 ± 0.9
EMAE	168.38	−17.05	N238.7 ± 0.6	88.3 ± 1.0	N163.2 ± 2.1	31.3 ± 1.0
Efate						
UTAN	168.32	−17.43	N244.6 ± 1.0	86.4 ± 1.4	N165.8 ± 4.6	21.0 ± 1.4
MGAL	168.2	−17.64	N246.1 ± 1.2	90.3 ± 2.3	N178.2 ± 5.9	20.3 ± 1.4
VILA[b]	168.32	−17.73	N244.9 ± 0.1	92.2 ± 0.3	N179.5 ± 1.5	23.1 ± 0.4
EFAT	168.56	−17.78	N244.2 ± 0.3	94.2 ± 0.6	N182.5 ± 1.7	25.3 ± 0.6
Erromango/Tanna/Aneytum/Futuna-Iti						
DILB	169.02	−18.82	N246.7 ± 0.7	117.3 ± 1.7	N219.5 ± 2.5	40.4 ± 1.8
ANIW	169.6	−19.24	N245.8 ± 1.1	117.2 ± 3.0	N217.5 ± 4.1	42.0 ± 2.8
TANA	169.25	−19.53	N247.6 ± 0.5	123.4 ± 1.3	N226.6 ± 1.7	46.4 ± 1.5
FTNV	170.23	−19.52	N257.8 ± 1.2	92.3 ± 2.7	N240.7 ± 13.4	11.2 ± 3.0
YTUM	169.77	−20.14	N248.5 ± 1.0	122.3 ± 2.5	N228.2 ± 3.2	45.4 ± 2.6

[a]See Table 2.
[b]Permanent site.

cially, for which the velocity is still poorly determined (see above) exhibits a much larger divergence rate with respect to the PP. This result indicates 84 ± 41 mm a^{-1} of divergence motion in the NE-SW direction (N52 ± 28°) at 11.7°S between PP and the northern Vanuatu arc. It confirms the hypothesis of a back-arc accretion zone at the rear of the northern Vanuatu segment, along which the spreading rate increases northward and ranging from 36 to 55 to 70–

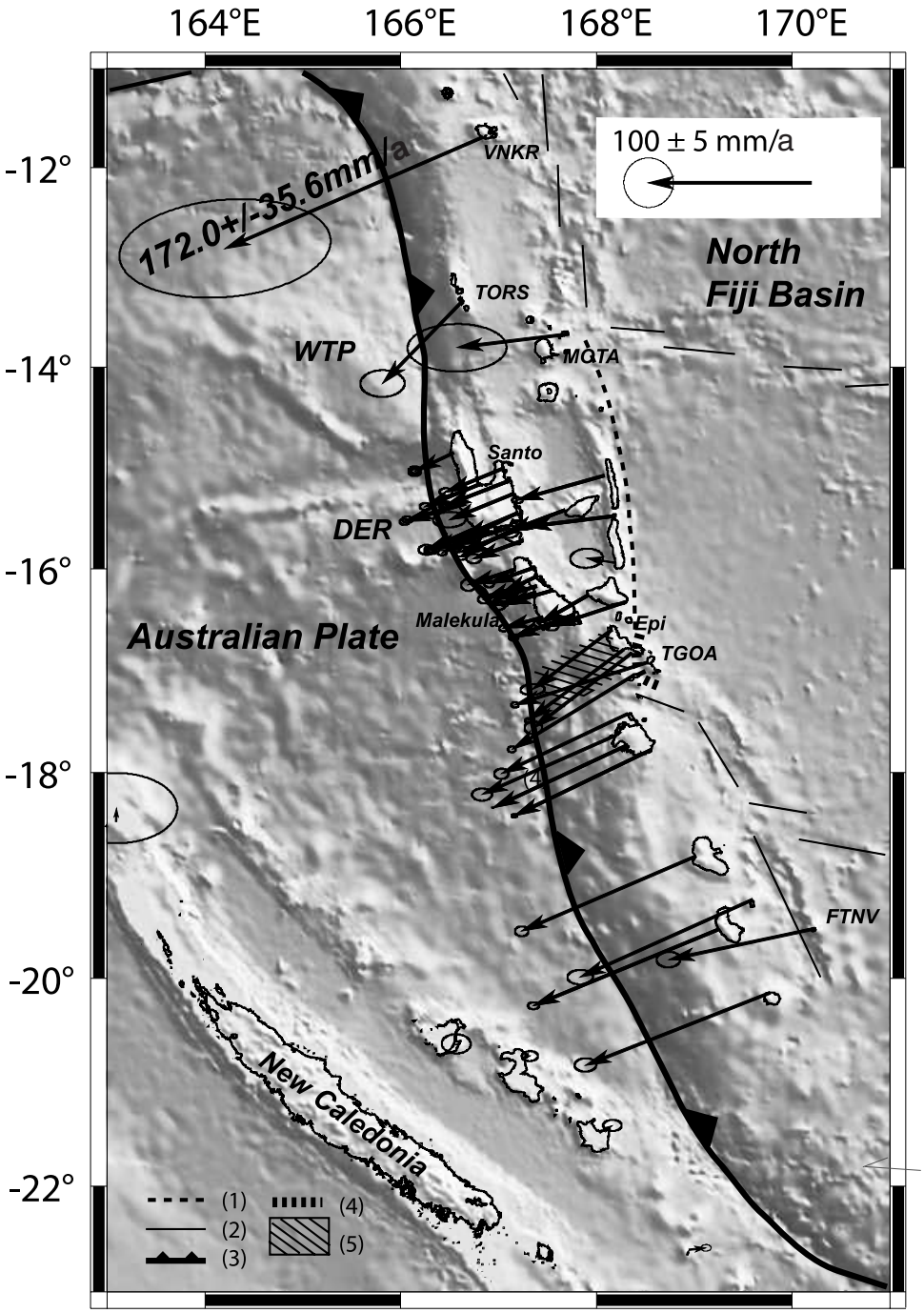

Figure 6. Horizontal interseismic GPS velocities for the VSZ in an Australia-fixed reference frame. The Australian motion is estimated as a rigid rotation from our GPS results with a least squares inversion. Abbreviations are as follows: WTP, West Torres Plateau; DER, D'Entrecasteaux Ridge. Lines are (1) BATB, (2) spreading ridge, (3) VSZ, (4) discontinuity supposed between TGOA and Epi island, and (5) transition zone.

81 mm a^{-1} as estimated by previous studies [*Pelletier and Louat*, 1989; *Pelletier et al.*, 1998; *Calmant et al.*, 2003]. In contrast, south of the northern Vanuatu back-arc extension, the converging motion of the Banks and Torres islands (13 to 14°S) relative to the NFB is probably controlled by the WTP collision. Finally, it must be noted that geodynamic models [*Pelletier and Louat*, 1989; *Pelletier et al.*, 1998] suggest that the Banks and Torres Islands movements are largely controlled by back-arc compression and therefore depart from the Vanikoro case. Clearly data from more observation sites are needed to further describe the deformation in the northern part of the Vanuatu arc.

[30] We assume now that the central segment (Santo, Malekula and the Aoba Basin) and the southern segment (Epi/Tongoa to Aneytum) behave as independent rigid blocks. We calculate rigid block rotations for these two sets

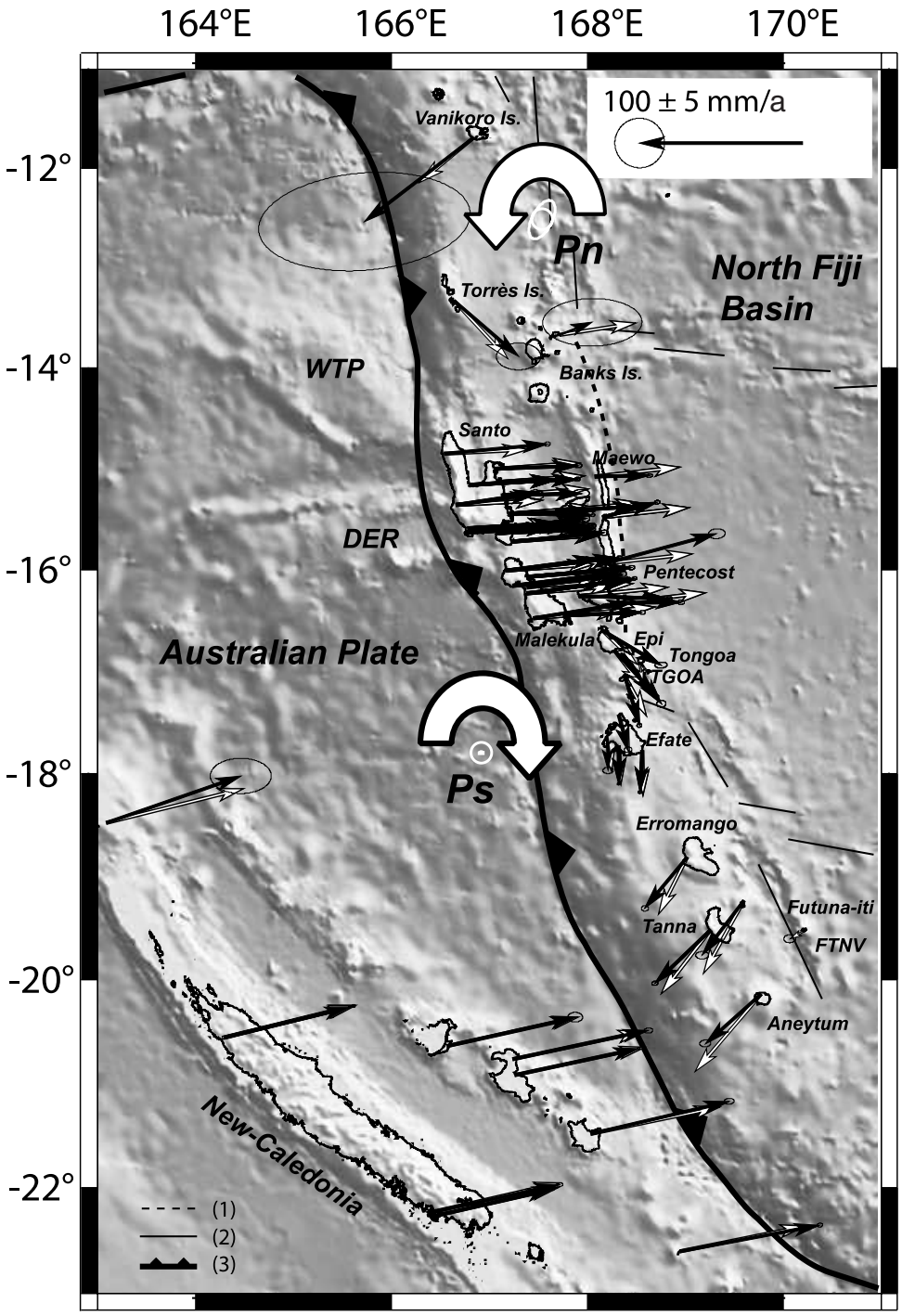

Figure 7. Horizontal interseismic velocities for the VSZ in a Pacific plate (PP)-fixed reference frame, from GPS (black) and modeled block motion (white). Error ellipses represent 2σ uncertainty. This rigid rotation is estimated from our GPS results with a least squares inversion. The large arrows represent the block motions along the central BATB. Abbreviations are as follows: WTP, West Torres Plateau; DER, D'Entrecasteaux Ridge; Pn and Ps, Euler poles for north block and south block, respectively. Lines are (1) BATB, (2) spreading ridge, and (3) VSZ.

of stations using a least squares inversion. The corresponding Euler Poles and rotation rates are given in Table 4.

[31] The central block motion is well constrained (by 28 stations) and fits the rigid block hypothesis at first order (Table 5). Differences between the GPS and modeled velocities are smaller in Santo and Malekula (that is for the sites close to the trench) than for the sites close to the back-arc thrust belt (Maewo and Pentecost) with 20 mm a^{-1} residuals. Consequently, the rigid block hypothesis is not

Table 4. Euler Pole Determination Fitting the GPS Velocities on the Vanuatu Subduction Zone With Respect to the Pacific Plate[a]

Longitude (deg)	Latitude (deg)	Ω (deg Ma^{-1})	σΩ (deg Ma^{-1})	Maximum	Minimum	Azimuth
			Pc			
165.29	**10.54**	**1.08**	**0.09**	**3.18**	**0.06**	**355.59**
167.44	−8.26	3.9	0.5	1	0.07	0
			Ps			
166.92	**−17.80**	**−8.97**	**0.14**	**0.04**	**0.02**	**263.69**
166.56	−18.39	−6.29	0.3	0.1	0.06	270
			Pn			
167.54	**−12.51**	**20.79**	**4.95**	**0.42**	**0.20**	**26.75**
166.91	−14.52	10.16	0.6	0.12	0.06	0

[a]This study (boldface) and from *Calmant et al.* [2003] (nonbold). Abbreviations are as follows: Pc, central block; Ps, south block; Pn, north block.

acceptable to explain the central arc interseismic velocities variations and active deformation may affect the central part of the arc. We will focus on this part of the arc in next sections.

[32] In the southern part, the GPS derived motion also fits the rigid block rotation model (although not as well as in the central block) confirming to a first order our hypothesis of a unique rotating block extending from Epi to Aneytum (Figure 7). Most of the twelve sites velocities are well constrained from long time series and more than six epochs of measurements. The Euler Pole is located on the AP, west of the Efate Island, and the block rotates clockwise at a rate of 8.97 ± 0.14 ° Ma^{-1}. The discrepancy between modeled and observed directions varies regularly from north to south (Figure 7), suggesting a continuous deformation throughout this block.

[33] The boundary zone between the central and south blocks is indicated by shallow earthquakes with strike-slip focal mechanisms [*Louat and Pelletier*, 1989; *Taylor et al.*, 1995; *Calmant et al.*, 2003]. Two of the six focal mechanism solutions (CMTS) have a thrust component. The location of these events varies by up to 50 km between different catalogs: in the NEIC, they are located south of Ambrym, west of Epi and on southern Epi, whereas in the CMTS catalog, they are mainly located east and southeast of Ambrym and east of Epi. Our boundary zone direction agrees with the azimuths of the pure strike-slip focal mechanism solutions if the ENE to EW nodal plane is chosen (slip vectors at 60°E for the events located immediately south of Ambrym and 90°E for the solutions east to southeast of Ambrym and west of Epi (see *Taylor et al.* [1995, Figure 2], *Calmant et al.* [2003, Figure 8], or *Lagabrielle et al.* [2003] for focal mechanisms location and solutions). This confirms the existence of a wide zone (transition zone in Figure 6) that accommodates the rapid variation of convergence motion relative to the NFB. From the estimated interseismic velocities at GPS stations close to Ambrym, South Malekula and Emae this zone undergoes a right lateral strike-slip movement of 26 ± 1 mm a^{-1} normal to the trench (direction N70°).

[34] To test our hypothesis that the easternmost sites (FTNV (Futuna-Iti) and TGOA (Tongoa)) behave like the NFB or PP, we assess the residuals of their GPS velocities with respect to the PP (Table 3). In Futuna-Iti, the velocity residual is 11 ± 3 mm a^{-1} directed N241 ± 13° while in Tongoa, the magnitude of the residual is 11 ± 1 mm a^{-1}, and the orientation is N169 ± 5°. These small residual velocities confirm that these two islands belong to the NFB and that the spreading rate between the NFB and the PP is negligible

Table 5. Residuals of the GPS Horizontal Velocities in Vanuatu Central Block With Respect to the Euler Pole Best Fit Rigid Rotation[a]

Sites	Longitude (deg)	Latitude (deg)	Direction (deg)	Residual (mm a^{-1})
		Santo/Malo		
NWST	166.54	−14.85	N74.28 ± 2.92	15.1 ± 1.7
WUSI	166.66	−15.36	N341.64 ± 8.85	4.9 ± 0.9
TGWS	166.66	−15.36	N303.49 ± 4.37	7.2 ± 1.3
LISB	166.77	−15.63	N66.19 ± 6.55	5.8 ± 1.8
TASM	166.9	−15.61	N99.63 ± 6.38	5.4 ± 1.2
AVNA	167.09	−15.64	N106.07 ± 8.12	4.8 ± 1.7
RATA	167.09	−15.6	N17.34 ± 20.31	2.8 ± 1.9
RATU	167.19	−15.62	N251.67 ± 27.8	2.4 ± 2.1
MALO	167.25	−15.72	N60.56 ± 18.85	3.1 ± 2.3
SANC	167.2	−15.45	N203.06 ± 13.49	1.9 ± 0.9
SHRK	167.14	−15.26	N236.58 ± 18.00	5.3 ± 4.1
HOGB	167.1	−15.13	N242.59 ± 8.44	4.9 ± 1.8
EKAR	167.06	−15	N203.87 ± 27.33	2.3+/2.1
BIGB	166.82	−15.16	N100.62 ± 51.46	1.1 ± 2.1
		Aoba		
AOBA	167.68	−15.42	N222.46 ± 27.97	3.4 ± 3.2
		Maewo/Pentecost		
MAWO	168.08	−15.08	N254.84 ± 1.72	17.3 ± 1.7
PNCT	168.16	−15.48	N279.57 ± 1.58	17.9 ± 1.3
WALI	168.18	−15.94	N50.61 ± 5.50	19.9 ± 4.3
		Malekula		
TNMR	167.17	−16.01	N42.57 ± 13.33	5.4 ± 2.3
LMBU	167.39	−16.17	N52.16 ± 8.19	5.9 ± 1.8
LVMP	167.24	−16.16	N65.32 ± 5.08	9.4 ± 2.1
MLKL	167.78	−16.45	N246.44 ± 4.65	7.8 ± 0.9
NSUP	167.4	−16.07	N82.00 ± 3.51	9.3 ± 2.3
RNSR	167.56	−16.21	N24.69 ± 11.42	3.4 ± 1.4
SWBY	167.45	−16.48	N49.89 ± 5.09	7.7 ± 1.4
VMVS	167.38	−16.23	N62.96 ± 5.84	8.7 ± 2.3
WLRN	167.37	−15.99	N59.65 ± 9.18	3.8 ± 2.1
		Ambrym		
ULEI	168.3	−16.33	N248.95 ± 2.70	16.3 ± 1.8
AMBR	167.92	−16.26	N173.88 ± 6.14	7.1 ± 0.8

[a]See Table 4.

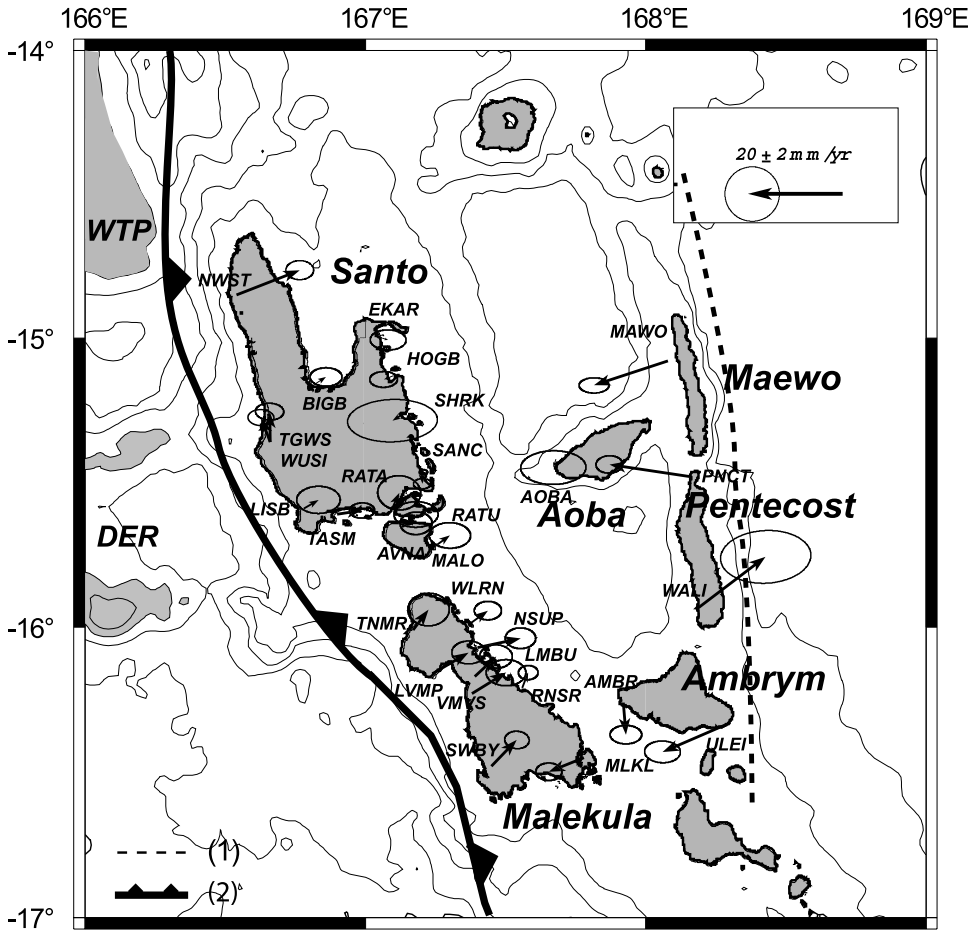

Figure 8. Horizontal GPS interseismic residuals for the Vanuatu central area with respect to a rigid block motion. This block motion is estimated as a rigid rotation from our GPS results with a least squares inversion. Ellipses represent 2σ uncertainty. Abbreviations are as follows: WTP, West Torres Plateau; DER, D'Entrecasteaux Ridge. Lines are (1) BATB and (2) VSZ.

at first order with respect to the Australian/Pacific relative plate motion. In addition, by comparing velocities on Futuna-Iti (FTNV) and Tanna (TANA) on the one hand and Tongoa (TGOA) and Emae (EMAE) on the other hand, we calculate the southern Vanuatu back-arc extension rate to be about 35 mm a^{-1} oriented N30° at 19.5°S and 20 mm a^{-1} oriented N350° at 17°S (Table 3). The inferred rate of back-arc extension increases southward, in good agreement with the morphology of the back-arc troughs that are more developed in south (Futuna Trough) than in the north (Vate Trough) (see Figure 1 for location).

4.3. Central Vanuatu: Intra-Arc Deformation, Back-Arc Shortening

[35] Previous studies of seismicity [*Isacks et al.*, 1981; *Louat et al.*, 1988; *Régnier et al.*, 2003], neotectonics [*Taylor et al.*, 1980, 1985, 1987, 1990; *Lagabrielle et al.*, 2003], marine geology and geophysics [*Collot et al.*, 1985; *Pelletier et al.*, 1994], kinematics [*Louat and Pelletier*, 1989; *Pelletier and Louat*, 1989; *Pelletier et al.*, 1998], and geodesy [*Taylor et al.*, 1995; *Calmant et al.*, 1995, 2003] revealed a very strong coupling at the interface between the central Vanuatu overriding margin and the subducting plate as well as back-arc shortening. The reduced convergence at the plate boundary, the disappearance of the trench, the uplift of the western and eastern belts, and the presence of the back-arc thrust zone are believed to be due to the DER entering into subduction [e.g., *Collot et al.*, 1985; *Pelletier and Louat*, 1989; *Pelletier et al.*, 1994, 1998; *Taylor et al.*, 1995].

4.3.1. The Horizontal Velocity Field

[36] The interseismic convergence rate estimated at the trench ranges between 25 (Malekula) and 43 ± 1 mm a^{-1} (west Santo) oriented N250 ± 5° (see Table 3). As already demonstrated by *Calmant et al.* [2003], these convergence rates are smaller than the shortening rates with respect to the NFB (or PP), which are in the range of 45 to 63 ± 1 mm a^{-1}, directed N84 ± 2°. This confirms the role of the central Vanuatu west dipping back-arc thrust as the major tectonic element in the Vanuatu convergence process and suggests the possible initiation of subduction polarity reversal along the eastern edge of the eastern belt [*Régnier et al.*, 2003].

[37] We now discuss velocity residuals with respect to rigid block rotation hypothesis (Table 5 and Figure 8) in order to detect nonrigid deformation through the central part of the arc. Residuals larger than 2σ represent a 95% significant discrepancy with respect to this rigid block hypothesis. Most of these velocity residuals point toward

Table 6. GPS Vertical Velocities for the Sites of the Vanuatu Central Block[a]

Site	Longitude (deg)	Latitude (deg)	Vertical Rate (mm a^{-1})
		Santo/Malo	
NWST	166.54	−14.85	4.7 ± 2.8
WUSI	166.66	−15.36	5.4 ± 2.8
TGWS	166.66	−15.36	2.3 ± 1.8
LISB	166.77	−15.63	11.4 ± 2.6
TASM	166.9	−15.61	8.4 ± 2.4
AVNA	167.09	−15.64	−5.6 ± 4.4
RATA	167.09	−15.6	−0.9 ± 5.8
RATU	167.19	−15.62	−2.7 ± 4.4
MALO	167.25	−15.72	1.1 ± 4.4
SANC	167.2	−15.45	−2.6 ± 0.6
SHRK	167.14	−15.26	8.9 ± 7.6
HOGB	167.1	−15.13	−12.4 ± 2.8
EKAR	167.06	−15	5.7 ± 3.8
BIGB	166.82	−15.16	4.5 ± 3.4
		Aoba	
AOBA	167.68	−15.42	11.9 ± 5.6
		Maewo/Pentecost	
MAWO	168.08	−15.08	−0.7 ± 2.6
PNCT	168.16	−15.48	−1.9 ± 2.6
WALI	168.18	−15.94	−4.3 ± 5.2
		Malekula	
TNMR	167.17	−16.01	−10.5 ± 4.6
LVMP	167.24	−16.16	−8.6 ± 3.4
VMVS	167.38	−16.23	−3.6 ± 4.2
SWBY	167.45	−16.48	−1.5 ± 2.6
MLKL	167.78	−16.45	−2.2 ± 2.6
RNSR	167.56	−16.21	−2.4 ± 2.2
LMBU	167.39	−16.17	−1.4 ± 4.1
NSUP	167.4	−16.07	−3.7 ± 3.4
WLRN	167.37	−15.99	−4.2 ± 3.0
		Ambrym	
AMBR	167.92	−16.26	2.8 ± 3.0
ULEI	168.3	−16.33	−10.9 ± 4.1

[a]Uncertainty is 2σ.

the central part of the basin, emphasizing that compressive deformation occurs in the central Vanuatu area. The largest residuals are observed along the central segment of the BATB (eastern belt), in Maewo and Pentecost islands. There, the shortening rate reaches 17 to 20 ± 1 mm a^{-1}, oriented N270 ± 10°). We observe no convergence between Aoba volcanic island, in the center of the IAB, and the Santo eastern coast. This clearly indicates, as previously noted using geological data [*Daniel et al.*, 1989; *Pelletier et al.*, 1994] that the shortening affects only the eastern part of the Aoba Basin. Yet Aoba Island is an active volcano that is probably subject to volcanically induced deformation. The high rate of residuals we observe along the eastern belt confirms the locking of the Maewo and Pentecost segment of the BATB as suggested by *Calmant et al.* [2003]. Even though no major (M_w 7 or above) earthquake has yet been recorded in this part of the central block since 1976 from global seismic data catalogs (e.g., NEIC or CMTS), such an event is likely to occur in the next decades to unlock this portion of the back-arc thrust zone, similar to the Ambrym 1999, M_w 7.5 earthquake that released the stress in the southern segment of the BATB [*Pelletier et al.*, 2000; *Lagabrielle et al.*, 2003; *Régnier et al.*, 2003]. It is possible that the motion of the Ambrym (AMBR and ULEI) and south Pentecost (WALI) sites located at the SE termination of the Aoba Basin is influenced by the post seismic deformation of 1999 Ambrym earthquake. The residuals at these sites are too uncertain to be interpreted, but Malekula Island's southernmost site (MLKL) displays a residual consistent with the Ambrym stations.

[38] The residuals in the southern part of Santo and on Malekula Islands are consistent with a mean rate of 8 ± 2 mm a^{-1} pointing N50 ± 20°. This residual motion, although small, is well constrained (more than 95% significance) and generally increases from the southernmost Santo to south Malekula, suggesting a block rotation or progressive deformation of the area, and a high coupling and locked interface in the south (below west and southwest Malekula). The residuals of the sites in central Santo are negligible except at Wusi (western coast) where the two collocated GPS stations give consistent velocity residuals of 6.1 ± 0.9 mm a^{-1} toward the north. This local motion toward the north can be related to the high coupling of the northern chain of the DER that interacts with the arc at the latitude of Wusi. Indeed the slight obliquity of the DER with the plate convergence motion implies a small component of motion parallel to the arc, the sweeping northern ridge asperities of the DER may affect the velocity field at this latitude.

[39] The northernmost site on Santo (NWST at the NW end of the Island) exhibits a significant residual of 15.1 ± 1.7 mm a^{-1} pointing N74 ± 3°. This velocity, if confirmed (it is based on three measurement epochs) suggests high coupling at the subduction interface that could be related to the subduction of the WTP entering the trench in the northern Santo Peninsula region.

4.3.2. The Vertical Velocity Field

[40] The vertical velocity field (Table 6 and Figure 9) and the horizontal residual velocities indicate how the central Vanuatu block deforms. The southeastern part of Santo, south Santo small Islands and Malekula Island show a coherent pattern of subsidence at rates from −1 ± 2 to −10 ± 2 mm a^{-1}. These rates are highest in the northwestern part of Malekula (at the TNMR and LVMP sites close to the trench) where they average −10 ± 3 mm a^{-1}. In other parts of Malekula to the southeastern part of Santo, the average subsidence rate is −2.5 ± 1 mm a^{-1}. In general, subsidence increases westward, toward the Vanuatu trench.

[41] Along the western coast of central and south Santo, we observe a general uplift with velocities between 2 and 11 mm a^{-1}, with the maximum values at the southwestern tip of Santo. At Wusi, the two collocated stations show consistent uplift with rates of 5 ± 3 mm a^{-1} and 2 ± 2 mm a^{-1}.

[42] Our measurements indicate a subsidence of −5 ± 3 mm a^{-1} at the northwestern tip of Santo. Except at the eastern tip of Ambrym where large subsidence (−11 ± 4 mm a^{-1}) is probably related to post seismic motion after the Ambrym 1999 large earthquake, we do not find any evidence for significant vertical displacement along the eastern belt. However, results indicate very slow subsidence or no motion (rates of −2 ± 3 mm a^{-1} and −4 ± 5 mm a^{-1} in Pentecost, −1 ± 3 mm a^{-1} in Maewo).

[43] In Aoba itself, we note a strong uplift of 12 ± 6 mm a^{-1} which is probably not related to tectonic activity,

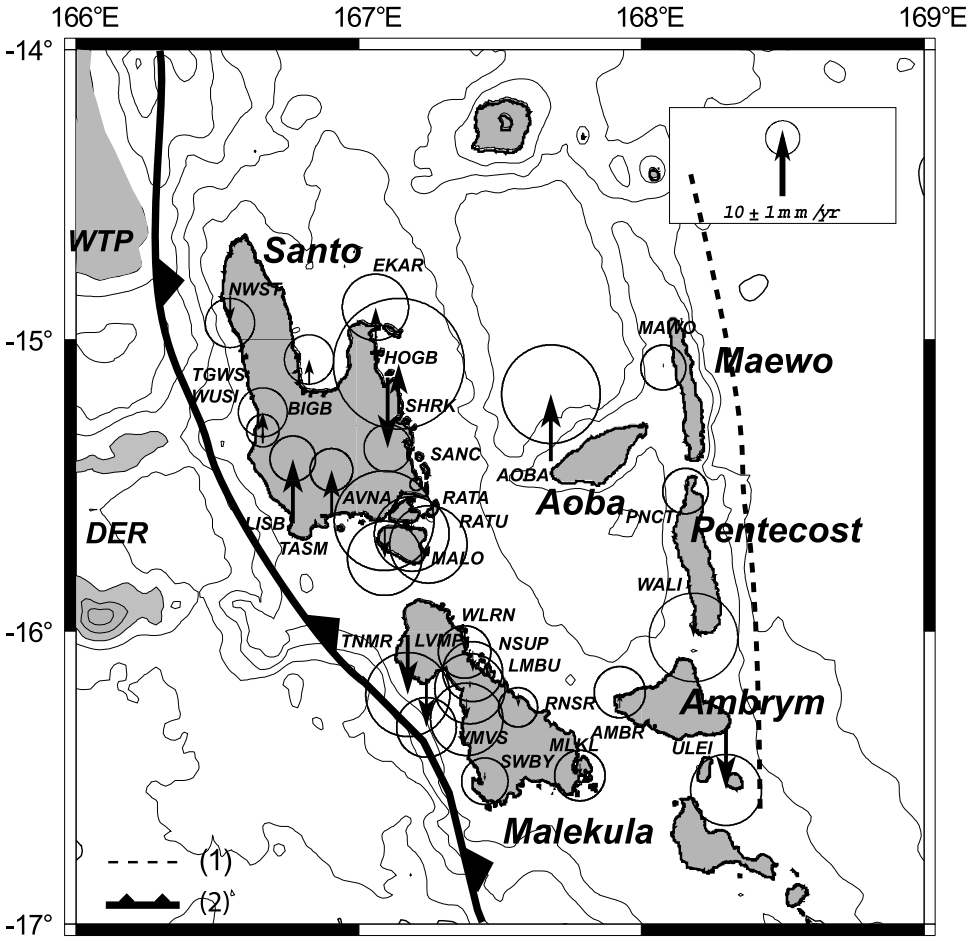

Figure 9. Vertical GPS interseismic velocities for the Vanuatu central block. Ellipses represent 1σ uncertainty. Abbreviations are as follows: WTP, West Torres Plateau; DER, D'Entrecasteaux Ridge. Lines are (1) BATB and (2) VSZ.

but rather to volcanically induced deformation (the last major volcanic event occurred in December 2005).

4.4. Locked Zone Modeling

[44] The surface deformation can be explained by a locked zone that couples the subducting plate to the overriding margin. We use the back slip elastic model of *Savage* [1983] and the mathematical expression of *Singh and Rani* [1993] to infer the location and parameters of this locked zone as well as the long-term convergence rate between the AP and the central part of the Vanuatu arc (Figure 10). The resulting motion of such a model is a thrust displacement on the deepest part of the subducting interface and a locked zone nearer to the trench. The strain accumulates on this locked zone before being released by a major seismic event. The model predicts shortening all along a horizontal transect normal to the trench on the overriding plate, with an inflexion point marking the downdip edge of the locked zone. On the vertical component, the downdip edge of the locked zone corresponds to a maximum uplift while the region close to the trench subsides. This model accounts for purely elastic deformation only and cannot explain any topography building. Three parameters have to be estimated: the long-term convergence rate, the dip and the width of the locked zone. The long-term convergence rate between the central part of the Vanuatu arc and the AP varies between 49 and 70 mm a^{-1} according to previous studies [e.g., *Taylor et al.*, 1995, 2005]. Regarding the geometric parameters of the locked zone, the aftershocks of the Santo earthquake, 2000, M_w 6.9, provide a priori information about the length and dip of the locked zone. The deeper edge of the rupture of the earthquake is located 30 km deep, under the east coast of Santo Island (M. Régnier, unpublished data, 2003). From those a priori informations, we investigated several values for each three model parameters (up to 70 tests) to theoretically compute the vertical and horizontal velocities due to the locked zone: 45 to 70 mm a^{-1} for the long-term convergence rate between the AP and the central Vanuatu arc facing the colliding ridge; 20 to 30° for the dip and 40 to 80 km for the width of the locked zone. We computed the RMS between modeled and observed GPS velocities to evaluate the quality of the fit. We used our horizontal interseismic velocities with respect to the AP and absolute vertical velocity fields to infer the locked zone parameters (namely, the edge, the dip angle, and the convergence rate). We then projected our GPS derived interseismic vertical and horizontal velocities onto two transects trending N70° (the mean convergence direction): The A-A′ transect, located 100 km south of the DER subduction/collision, and the B-B′ tran-

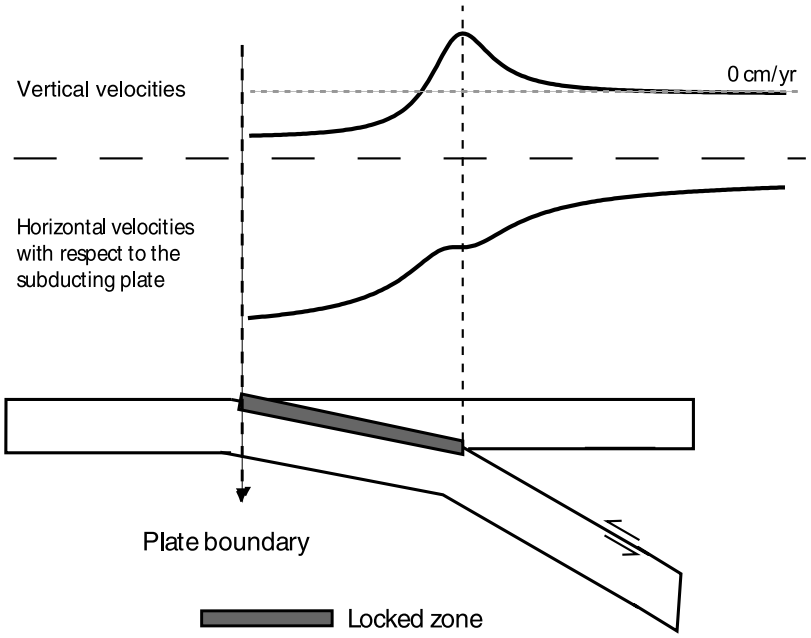

Figure 10. Sketch of the interseismic strain accumulation model from *Savage* [1983], in a locked zone. (top) Vertical and (middle) horizontal velocity model on a transect perpendicular to the trench, born by the (bottom) locked zone.

sect facing the DER (Figure 11). The A-A′ transect includes stations up to 40 km off the transect line (nine sites, including west Ambrym AMBR but not east Ambrym ULEI). The B-B′ transect comprises sites up to 25 km off-line (nine sites in south Santo, Aoba, Maewo and Pentecost). Assuming that the locked zone is characterized by the same parameters along the central part of the Vanuatu arc, the best fit between modeled and observed velocities on horizontal and vertical components for the two transects is obtained for a mean long-term convergence rate of 54 mm a^{-1} and mean geometric parameters of 25° dip and 50 km width for the locked zone (Figure 12).

[45] Along the A-A′ transect (Figure 12), the modeled horizontal velocities closely agree with the observations (3.5 ± 4.3 mm a^{-1} on average). Vertical component, discrepancies reach 9.7 mm a^{-1} with an average of 3.9 ± 5.0 mm a^{-1}. The subsidence of Malekula Island measured during this interseismic stage is well explained by a locked zone ending at a depth of 20 km below the western coast of Malekula. Facing the DER collision (B-B′ transect) the modeled versus measured motions differ by 0.1 to 10.7 mm a^{-1} (mean of 3.7 ± 5.0 mm a^{-1}) on the horizontal component and from 1.0 to 22.1 mm a^{-1} on the vertical (mean difference of 8.6 ± 10.4 mm a^{-1}). A closer look at the horizontal and vertical velocity transects reveals some characteristic patterns. On the horizontal component, the agreement between the modeled and measured motions is generally good (0.1 to 4 mm a^{-1}) except within the eastern belt. The high shortening rates we observe in Maewo and Pentecost cannot be explained by the single locked zone model. For those two stations, the differences between modeled and observed velocities on horizontal component are significant (9.2 ± 2.1 mm a^{-1}) and confirm that significant strain accumulation and coupling is taking place along the BATB.

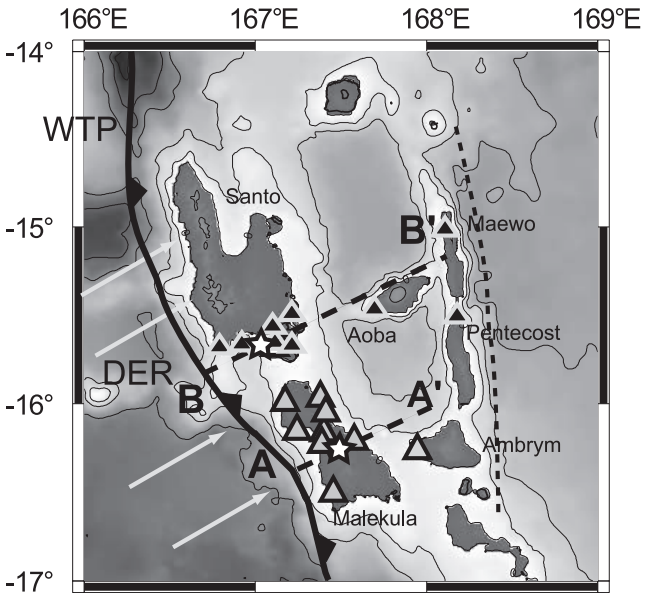

Figure 11. Transects and GPS stations used to assess the locked zone parameters in this study. Shaded triangles represent the A-A′ (TNMR, LVMP, LMBU, WLRN, SWBY, VMVS, NSUP, RNSR, and AMBR) transect GPS stations, and solid triangles represent the B-B′ transect GPS stations (LISB, TASM, AVNA, RATA, RATU, SANC, AOBA, PNCT, and MAWO). The bold lines represent the A-A′ and B-B′ transects. The white arrows show the convergence direction. Abbreviations are as follows: DER, D'Entrecasteaux Ridge; WTP, Wet Torres Plateau. The stars indicate the edge of the locked zone as deduced from the GPS velocity interpretation (Figure 12). Lines are (1) BATB and (2) VSZ.

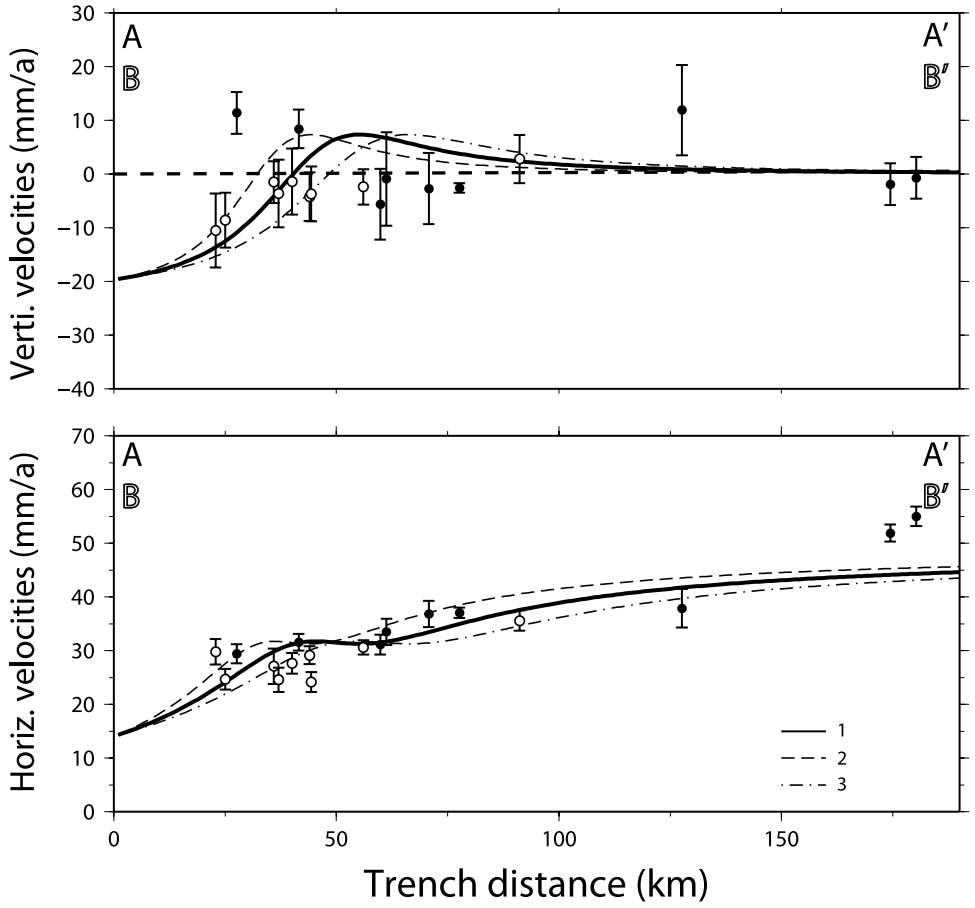

Figure 12. (top) Vertical and (bottom) horizontal (perpendicular to the trench) velocity profiles for the GPS stations of the A-A′ (open circle) and B-B′ (filled circle) transects. Distances are given with respect to the trench. The bold curves represent the best fit of the locked zone and long-term convergence rate model (dip, 20°; width, 50 km; slip, 54 mm a^{-1}) estimated from observed velocities. Lines 2 and 3 represent the effect of the width variation in the model (45 and 60 km, respectively). See Figure 11 for the transect location.

[46] Concerning the vertical velocities along this B-B′ transect, the poor fit we obtain is improved if we exclude the Aoba volcanic site, located at the center of the IAB and displaying a strong uplift which is likely related to volcanic activity. Even so, the discrepancies remain high at the two sites located along the southwest Santo coast. In this part of the Santo island significant uplift are estimated (9.9 ± 2.1 mm a^{-1}) whereas the model predicts subsidence approaching the trench. These positive vertical velocities close to the trench could be explained by the DER entering into subduction facing the B-B′ transect. The subduction of the ridge is not accounted in the used model and may be responsible for anelastic strain (positive rebound due to detachment of slab in response to the ridge subduction [*Chatelain et al.*, 1992]). In addition, large active uplift in western Santo is evidenced by steep relief, late Quaternary-Holocene reef terraces, large normal faults scarps facing the sea along the western coast of Santo and the steep relief observe in Santo with many normal fault scarps around the southwest coast.

[47] To conclude, we note that the locked zone characteristics (25° dip angle, 50 km extent, 20 km maximum depth) fit observations along the transect A-A′ rather well and fit observations along the transect B-B′ to the first order. Future works with more data at the east of the central part of the arc and a better constrain on BATB geometric characteristics will improve the present model.

5. Conclusion

[48] We obtain horizontal velocities along the Vanuatu arc and a 3-D velocity filed over the central Vanuatu arc that is derived from 15 years of GPS surveys and is based on measurements at more than 45 stations. The horizontal velocities with respect to the AP show convergence vectors normal to the trench with large magnitude variations from north to south. We confirm the results of *Calmant et al.* [2003], which split the arc into three main domains: the northern, central, and southern blocks. The highest convergence rate is found in the far north station of Vanikoro (172 ± 36 mm a^{-1}) and agrees well with geodynamic predictions of 150 to 170 mm a^{-1} [*Pelletier and Louat*, 1989; *Pelletier et al.*, 1998]. The lowest rates (27 to 43 mm a^{-1}) are found in the central block opposite the DER collision/subduction. Motions expressed relative to the NFB (or PP) confirm the arc partitioning, with blocks

rotating independently. The northern block rotates anticlockwise in relation with rapid back-arc spreading, estimated to be 84 ± 41 mm a^{-1} orientation NE-SW at the latitude of Vanikoro Island. This result is in good agreement with the geodynamic prediction of 55 to 80 mm a^{-1} [*Pelletier and Louat*, 1989; *Pelletier et al.*, 1998]. The central block translates eastward with rates relative to the NFB exceeding the convergence rates relative to the AP. This confirms that more convergence is accommodated at the eastern bound of the arc than at the Vanuatu trench. The southern block moves rapidly relative to AP (80 to 120 mm a^{-1}) and rotates clockwise relative to the NFB in relation with back-arc extension. The two easternmost sites within this southern block (at Futuna-Iti and Tongoa) exhibit velocities almost the same as the NFB motion, indicating back-arc opening at the rear of the Vanuatu archipelago at a rate of about 20 to 35 mm a^{-1} in a roughly NS to NNE-SSW direction.

[49] In the central block, residual horizontal rates show shortening rates close to 20 mm a^{-1} between the eastern belt (BATB) and the Aoba Island. Smaller but significant and consistent residuals at the southern coast of Santo and Malekula point toward the center of the IAB whereas no (or too small to be significant) residuals on the central-northern part of Santo (except the northwestern tip) indicates that this part moves consistently with the central block. The only exception is the northwestern tip of Santo that shows a significant residual (15 mm a^{-1}) also pointing eastward and suggesting the presence of a locked interface below northernmost Santo, in relationship with the entering of the WTP in the subduction.

[50] This partitioning between Malekula–southeast Santo, southwest-central Santo, and northwestern Santo is also observed in the vertical rates, with coherent subsidence on the southern part (Malekula and southeastern Santo), uplift on southwestern and central Santo and subsidence on northwestern most part of Santo. Elastic modeling of the interseismic stage deformation produced by a locked portion of subduction interface agrees well with measured vertical and horizontal velocities along a transect normal to the trench and south of the DER entering into subduction. A 50 km wide locked zone dipping 25° eastward and down to 20 km deep below the western coast of Malekula with a long-term convergence rate between the AP and the central part of the Vanuatu arc estimated to 54 mm a^{-1} are required to match the observations. Another transect, facing the DER, show large discrepancies for both the stations close to the trench and the stations on the back–arc eastern belt. However, we are confident that the characteristics of the locked zone we obtain are mainly correct, since the effect of the shape of the DER and back-arc thrust interface have not been taken into account in this modeling.

[51] **Acknowledgments.** This project was funded by the French program "DyETI" and the Institut de Recherche pour le Développement (IRD). We are grateful to the IRD for providing GPS data and logistical support (P. Lebellegard and J.-M. Devaux) and to the operators who helped us with the field observations (J.-L. Laurent, J.-M. Boré, and S. Deroussi). We are indebted to the Vanuatu Survey Department (M. Kalsale and J.-C. Willy) and to the Vanuatu Department for Geology, Mines, and Water Resources (E. Garaebiti) for logistical support and field operations. We would also like to thank the Direction des Infrastructures, de la Topographie et des Transports Terrestres/Bureau de Géodésie et de Nivellement (DITTT/BGN) of New Caledonia for logistical support and help during field operations as well as the Salomon Association (A. Le Breus). We also thank the IRD R/V *Alis* crew for their help in GPS coastal measurements. Detailed comments and suggestions of Jean-Marc Daniel, an anonymous reviewer, and the associate editor greatly contributed to the improvement of our article. This publication is supported by the ANR ARC-Vanuatu.

References

Altamimi, Z., P. Sillard, and C. Boucher (2002), ITRF2000: A new release of the International Terrestrial Reference Frame for earth science applications, *J. Geophys. Res.*, *107*(B10), 2214, doi:10.1029/2001JB000561.

Altamimi, Z., X. Collilieux, J. Legrand, B. Garayt, and C. Boucher (2007), ITRF2005: A new release of the International Terrestrial Reference Frame based on time series of station positions and Earth Orientation Parameters, *J. Geophys. Res.*, *112*, B09401, doi:10.1029/2007JB004949.

Auzende, J. M., B. Pelletier, and J. P. Eissen (1995), The North Fiji Basin: Geology, structure and geodynamic evolution, in *Back-Arc Basin: Tectonics and Magmatism*, edited by B. Taylor, pp. 139–175, Plenum, New York.

Beavan, J., P. Tregoning, M. Bevis, T. Kato, and C. Meertens (2002), Motion and rigidity of the Pacific Plate and implications for plate boundary deformation, *J. Geophys. Res.*, *107*(B10), 2261, doi:10.1029/2001JB000282.

Beutler, G., M. Rothacher, S. Schaer, T. Springer, J. Kouba, and R. Neilan (1999), The International GPS Service (IGS): An interdisciplinary service in support of Earth sciences, *Adv. Space Res.*, *23*, 631–635, doi:10.1016/S0273-1177(99)00160-X.

Blewitt, G., and O. Lavallée (2002), Effect of annual signals on geodetic velocity, *J. Geophys. Res.*, *107*(B7), 2145, doi:10.1029/2001JB000570.

Bourne, S., P. England, and B. Parsons (1998), The motion of crustal blocks driven by flow of the lower lithosphere and implications for slip rates of continental strike-slip faults, *Nature*, *391*, 655–659, doi:10.1038/35556.

Calmant, S., P. Lebellegard, F. W. Taylor, M. Bevis, D. Maillard, J. Recy, and J. Bonneau (1995), Geodetic measurements of convergence across the New Hebrides subduction zone, *Geophys. Res. Lett.*, *22*, 2573–2576, doi:10.1029/95GL01780.

Calmant, S., B. Pelletier, R. Pillet, M. Régnier, P. Lebellegard, D. Maillard, F. W. Taylor, M. Bevis, and J. Recy (1997), Interseismic and coseismic motions in GPS series related to the Ms 7.3 July 13, 1994, Malekula earthquake, central New Hebrides subduction zone, *Geophys. Res. Lett.*, *24*, 3077–3080, doi:10.1029/97GL02962.

Calmant, S., M. Berge-Nguyen, and A. Cazenave (2002), Global seafloor topography from a least-squares inversion of altimetry-based high-resolution mean sea surface and ship-board soundings, *Geophys. J. Int.*, *151*, 795–808, doi:10.1046/j.1365-246X.2002.01802.x.

Calmant, S., B. Pelletier, P. Lebellegard, M. Bevis, F. W. Taylor, and D. A. Phillips (2003), New insights on the tectonics along the New Hebrides subduction zone based on GPS results, *J. Geophys. Res.*, *108*(B6), 2319, doi:10.1029/2001JB000644.

Carney, J., and A. MacFarlane (1982), Geological evidence bearing on the Miocene to recent structural evolution of the New Hebrides arc, *Tectonophysics*, *87*, 147–175, doi:10.1016/0040-1951(82)90225-6.

Carney, J. N., A. MacFarlane, and D. I. J. Mallick (1985), The Vanuatu island arc: An outline of the stratigraphy, structure, and petrology, in *The Ocean Basins and Margins—The Pacific Ocean*, edited by E. M. Nairn et al., pp. 685–718, Plenum, New York.

Chatelain, J. L., P. Molnar, R. Prévot, and B. Isacks (1992), Detachment of part of the downgoing slab and uplift of the New Hebrides (Vanuatu) islands, *Geophys. Res. Lett.*, *19*, 1507–1510, doi:10.1029/92GL01389.

Chung, W.-Y., and H. Kanamori (1978), A mechanical model for plate deformation associated with aseismic ridge subduction in the New Hebrides, *Tectonophysics*, *50*, 29–40, doi:10.1016/0040-1951(78)90197-X.

Cloos, M. (1992), Thrust-type subduction-zone earthquakes and seamount asperities: A physical model for seismic rupture, *Geology*, *20*, 601–604, doi:10.1130/0091-7613(1992)020<0601:TTSZEA>2.3.CO;2.

Collot, J. Y., J. Daniel, and R. V. Burne (1985), Recent tectonics associated with the subduction/collision of the d'Entrecasteaux Zone in the central New Hebrides, *Tectonophysics*, *112*, 325–356, doi:10.1016/0040-1951(85)90185-4.

Collot, J. Y., et al. (1992), *Proceedings of the Ocean Drilling Program, vol. 134, Scientific Results*, Ocean Drill. Program, College Station, Tex.

Daniel, J., et al. (1989), Déformation compressive d'un bassin intra-arc dans un contexte de collision ride-arc: Le bassin d'Aoba, arc des Nouvelles-Hébrides, *C. R. Acad. Sci., Ser. II*, *308*, 239–245.

DeMets, C., R. G. Gordon, D. F. Argus, and S. Stein (1994), Effect of recent revisions to the geomagnetic reversal time scale on estimates of current plate motions, *Geophys. Res. Lett.*, *21*, 2191–2194, doi:10.1029/94GL02118.

Dubois, J., J. Launay, J. Recy, and J. Marshall (1977), New Hebrides trench: Subduction rate from associated lithospheric bulge, *Can. J. Earth Sci.*, *14*, 250–255.

Eanes, R., and A. Schuler (1999), An improved global ocean tide model from TOPEX/Poseidon altimetry: MCSR4.O, paper presented at the 24th General Assembly, Eur. Geophys. Soc., The Hague, Netherlands.

Geist, E. L., M. A. Fisher, and D. W. Scholl (1993), Large-scale deformation associated with ridge subduction, *Geophys. J. Int.*, *115*, 344–366, doi:10.1111/j.1365-246X.1993.tb01191.x.

Greene, H., et al. (1994), Vanuatu, covering Leg 134 of the cruises of the drilling vessel JOIDES Resolution, Port of Townsville, Queensland, Australia, to Suva, Republic of Fiji, sites 827–833, 11 October–17 December 1990, *Proc. Ocean Drill. Program Sci. Results*, *134*, 665 pp.

Isacks, B. L., R. K. Cardwell, J. L. Chatelain, M. Barazangi, J. M. Marthelot, D. Chinn, and R. Louat (1981), Seismicity and tectonics of the central New Hebrides island arc, in *Earthquake Prediction*, *Maurice Ewing Ser.*, vol. 4, edited by D. W. Simpson and P. G. Richards, pp. 93–116, AGU, Washington, D. C.

Jouannic, C., F. W. Taylor, A. L. Bloom, and M. Bernat (1980), Late Quaternary uplift history from emerged reef terraces on Santo and Malekula islands, central New Hebrides island arc, *Tech. Bull., 3*, pp. 91–108, Econ. and Soc. Comm. for Coord. for Jt. Prospect. for Miner. Resour. in S. Pac. Offshore Areas (CCOP/SOPAC), Suva, Fiji.

King, R., and Y. Bock (2003), Documentation for the GAMIT GPS software analysis, *Rel. 10.1*, Mass. Inst. of Technol. and Scripps Inst. of Oceanogr., Cambridge, Mass.

Lagabrielle, Y., B. Pelletier, G. Cabioch, M. Régnier, and S. Calmant (2003), Coseismic and long-term vertical displacement due to back arc shortening, central Vanuatu: Offshore and onshore data following the Mw 7.5, 26 November 1999 Ambrym earthquake, *J. Geophys. Res.*, *108*(B11), 2519, doi:10.1029/2002JB002083.

Larson, K. M., and D. C. Agnew (1991), Application of the Global Positioning System to crustal deformation measurements: part I. Precision and accuracy, *J. Geophys. Res.*, *96*, 16,547–16,566, doi:10.1029/91JB01275.

Louat, R., and B. Pelletier (1989), Seismotectonics and present-day relative plate motions in the New Hebrides–North Fiji Basin region, *Tectonophysics*, *167*, 41–55, doi:10.1016/0040-1951(89)90293-X.

Louat, R., M. Hamburger, and M. Monzier (1988), Shallow and intermediate depth seismicity in the New Hebrides arc: Constraints on the subduction process, in *Geology and Offshore Resources of Pacific Islands Arcs—Vanuatu Region*, *Earth Sci. Ser.*, vol. 8, edited by H. G. Greene and F. L. Wong, pp. 279–286, Circum. Pac. Counc. for Energy and Miner. Res., Houston, Tex.

MacFarlane, A., J. Carney, A. Crawford, and H. Greene (1988), Vanuatu: A review of the onshore geology, in *Geology and Offshore Resources of Pacific Islands Arcs—Vanuatu Region*, *Earth Sci. Ser.*, vol. 8, edited by H. G. Greene and F. L. Wong, pp. 45–91, Circum. Pac. Counc. for Energy and Miner. Res., Houston, Tex.

Mallick, D. I. J. (1975), Development of the New Hebrides Archipelago, *Philos. Trans. R. Soc. London, Ser. B*, *272*, 277–285, doi:10.1098/rstb.1975.0087.

McCarthy, D. D., and G. Petit (2004), IERS Conventions, *IERS Tech. Note 32*, 127 pp., Verl. des Bundesamts für Kartogr. und Geod., Frankfurt am Main, Germany.

Meffre, S., and A. Crawford (2001), Collision tectonics in the New Hebrides arc (Vanuatu), *Isl. Arc*, *10*, 33–50, doi:10.1046/j.1440-1738.2001.00292.x.

Mitchell, A., and A. Warden (1971), Geological evolution of the New Hebrides island arc, *J. Geol. Soc.*, *127*, 501–529, doi:10.1144/gsjgs.127.5.0501.

Niell, A. (1996), Global mapping functions for the atmosphere delay at radio wavelengths, *J. Geophys. Res.*, *101*, 3227–3246, doi:10.1029/95JB03048.

Nur, A. (1974), Matsushiro, Japan, earthquake swarm; confirmation of the dilatancy–fluid diffusion model, *Geology*, *2*, 217–221, doi:10.1130/0091-7613(1974)2<217:MJESCO>2.0.CO;2.

Pelletier, B., and R. Louat (1989), Mouvements relatifs des plaques dans le Sud-Ouest Pacifique, *C. R. Acad. Sci., Ser. II*, *308*, 123–130.

Pelletier, B., M. Meschede, T. Chabernaud, P. Roperch, and X. Zhao (1994), Tectonics of the central New Hebrides arc, North Aoba Basin, *Proc. Ocean Drill. Program Sci. Results*, *134*, 431–444.

Pelletier, B., S. Calmant, and R. Pillet (1998), Current tectonics of Tonga–New Hebrides region, *Earth Planet. Sci. Lett.*, *164*, 263–276, doi:10.1016/S0012-821X(98)00212-X.

Pelletier, B., et al. (2000), The Mw 7.5 November 26, 1999, Ambrym-Pentecost (Vanuatu) earthquake: Preliminary data on seismicity, associated tsunami and crustal motions, *C. R. Acad. Sci., Ser. IIA*, *331*, 21–28.

Régnier, M., S. Calmant, B. Pelletier, and Y. Lagabrielle (2003), The Mw 7.51999 Ambrym earthquake, Vanuatu: A back-arc intraplate thrust event, *Tectonics*, *22*(4), 1034, doi:10.1029/2002TC001422.

Saastamoinen, J. (1973a), Contributions to the theory of atmospheric refraction: part 1, *Bull. Geod.*, *105*, 279–298.

Saastamoinen, J. (1973b), Contributions to the theory of atmospheric refraction: part 2, *Bull. Geod.*, *106*, 383–397.

Saastamoinen, J. (1973c), Contributions to the theory of atmospheric refraction: part 3, *Bull. Geod.*, *107*, 13–34.

Savage, J. (1983), A dislocation model of strain accumulation and release at a subduction zone, *J. Geophys. Res.*, *88*, 4984–4996, doi:10.1029/JB088iB06p04984.

Savage, J., and W. Prescott (1978), Asthenosphere readjustment and the earthquake cycle, *J. Geophys. Res.*, *83*, 3369–3376, doi:10.1029/JB083iB07p03369.

Scholz, C., and C. Small (1997), The effect of seamount subduction on seismic coupling, *Geology*, *25*, 487–490, doi:10.1130/0091-7613(1997)025<0487:TEOSSO>2.3.CO;2.

Schutz, B., M. Bevis, F. W. Taylor, D. Kuang, P. Abusali, M. Watkins, J. Recy, B. Perin, and O. Peyroux (1993), The Southwest Pacific GPS Project: Geodetic results from Burst 1 of the 1990 Field Campaign, *J. Geod.*, *67*, 224–240, doi:10.1007/BF00806251.

Singh, S. J., and S. Rani (1993), Crustal deformation associated with two-dimensional thrust faulting, *J. Phys. Earth*, *41*, 87–101.

Taylor, F. W., B. Isacks, C. Jouannic, A. Bloom, and J. Dubois (1980), Coseismic and Quaternary vertical tectonic movements, Santo and Malekula Islands, New Hebrides island arc, *J. Geophys. Res.*, *85*, 5367–5381, doi:10.1029/JB085iB10p05367.

Taylor, F. W., C. Jouannic, and A. L. Bloom (1985), Quaternary uplift of the Torres Islands, northern New Hebrides frontal arc: Comparison with Santo and Malekula Islands, central New Hebrides frontal arc, *J. Geol.*, *93*, 419–438.

Taylor, F. W., C. Frohlich, J. Lecolle, and M. Strecker (1987), Analysis of partially emerged corals and reef terraces in the central Vanuatu arc: Comparison of contemporary coseismic and nonseismic with Quaternary vertical movements, *J. Geophys. Res.*, *92*, 4905–4933, doi:10.1029/JB092iB06p04905.

Taylor, F. W., R. Edwards, G. Wasserburg, and C. Frohlich (1990), Seismic recurrence intervals and timing of aseismic subduction inferred from emerged corals and reefs of the central Vanuatu (New Hebrides), *J. Geophys. Res.*, *95*, 393–408.

Taylor, F. W., et al. (1995), Geodetic measurements of convergence at the New Hebrides island arc indicate arc fragmentation caused by an impinging aseismic ridge, *Geology*, *23*, 1011–1014, doi:10.1130/0091-7613(1995)023<1011:GMOCAT>2.3.CO;2.

Taylor, F. W., et al. (2005), Rapid forearc uplift and subsidence caused by impinging bathymetric features: Examples from the New Hebrides and Solomon arcs, *Tectonics*, *24*, TC6005, doi:10.1029/2004TC001650.

Walpersdorf, A., E. Calais, J. Haase, L. Eymard, M. Desbois, and H. Vedel (2001), Atmospheric gradients estimated by GPS compared to a high resolution numerical weather prediction (NWP) model, *Phys. Chem. Earth, Part A*, *26*, 147–152, doi:10.1016/S1464-1895(01)00038-2.

V. Ballu and M. Diament, Equipe de Géophysique Spatiale et Planétaire, Institut de Physique du Globe de Paris, 4 place Jussieu, F-75252 Paris CEDEX 05, France.

N. Bergeot, Reference Systems and Geodynamic, Royal Observatory of Belgium, Avenue Circulaire, 3, 1180 Brussels, Belgium. (nicolas.bergeot@oma.be)

M. N. Bouin, Laboratoire de Recherches en Géodésie, IGN, Champs sur Marne, F-77455 Marne la Vallée CEDEX, France.

S. Calmant, Laboratoire d'Etudes en Géophysique et Océanographie Spatiales, UMR 5566, Observatoire Midi Pyrenées, CNRS, 14 Avenue E. Belin, F-31400 Toulouse, France.

B. Pelletier, Géosciences Azur, UMR 6526, Centre IRD Nouméa, 98848 Nouméa, New Caledonia.

M. Régnier, Géosciences Azur, UMR 6526, IRD, 250 avenue Albert Einstein, F-06560 Valbonne, France.